9-1-2015

Measurement of Interfacial Adhesion in Glass-Epoxy Systems Using the Indentation Method

Karen Hutchins

Karen Isabel Hutchins

Candidate

Mechanical Engineering

Department

This thesis is approved, and it is acceptable in quality and form for publication:

Approved by the Thesis Committee:

Tariq Khraishi, Chairperson

Mehran Tehrani

Rajan Tandon

MEASUREMENT OF INTERFACIAL ADHESION IN GLASS-EPOXY SYSTEMS USING THE INDENTATION METHOD

by

KAREN ISABEL HUTCHINS

B.S., PHYSICS, CALIFORNIA STATE UNIVERSITY SACRAMENTO, 2004
M.S., ASTRONOMY, SAN DIEGO STATE UNIVERSITY, 2006

THESIS

Submitted in Partial Fulfillment of the
Requirements for the Degree of

Master of Science
Mechanical Engineering

The University of New Mexico
Albuquerque, New Mexico

July, 2015

DEDICATION

This thesis is dedicated to my father. My hero. My rock. The one and only stable force throughout my life. Always there with a helping hand and words of encouragement. The man who taught me that quitting is not an option. I am eternally grateful for his unconditional love and support.

ACKNOWLEDGMENTS

Heartfelt thanks to my UNM advisor, Dr. Tariq Khraishi, for helping me to obtain an internship at Sandia National Laboratories. It was an amazing opportunity and I'll always be grateful for that. Thank you also to Dr. Rajan Tandon and Cory Gibson at Sandia National Laboratories for their excellent tutelage.

All experiments for this thesis were performed at Sandia National Laboratories in Albuquerque, NM. Sandia National Laboratories is a multi-program laboratory managed and operated by Sandia Corporation, a wholly owned subsidiary of Lockheed Martin Corporation, for the U.S. Department of Energy's National Nuclear Security Administration under contract DE-AC04-94AL8500. SAND2015-4881 T

MEASUREMENT OF INTERFACIAL ADHESION IN GLASS-EPOXY SYSTEMS USING THE INDENTATION METHOD

by

Karen Isabel Hutchins

B.S., Physics, California State University Sacramento, 2004

M.S., Astronomy, San Diego State University, 2006

M.S., Mechanical Engineering, University of New Mexico, 2015

ABSTRACT

The adhesion of coatings often controls the performance of the substrate-coating system. Certain engineering applications require an epoxy coating on a brittle substrate to protect and improve the performance of the substrate. Experimental observations and measurements of interfacial adhesion in glass-epoxy systems are described in this thesis. A comparison study of how different glass treatments affect adhesion was also conducted: smooth versus rough, clean versus unclean, stressed versus non-stressed. The Oliver and Pharr method was utilized to calculate the bulk epoxy hardness and elastic modulus. Spherical indentations were used to induce delaminations at the substrate-coating interface. The delamination sizes as a function of load were used to calculate the interfacial toughness. The interfacial fracture energy of my samples is an order of magnitude higher than a previous group who studied a similar glass-epoxy system.

TABLE OF CONTENTS

LIST OF FIGURES

LIST OF TABLES

1. Introduction

Coatings and bonded systems between different material groups (metals, ceramics, and polymers) and within each group are widely used. A few examples include: polymer coated dielectrics, encapsulated electronic packages, brazed and soldered assemblies, glass to metal seals, plated and coated electrical contacts, coatings on tribological materials, and arc-sprayed components. The fundamental property that describes the performance of a coating is its adhesion to the substrate. Adhesion failure is usually defined as a cracking/delamination event at the interface between the substrate and coating. There are four main mechanisms of adhesion: 1) mechanical interlocking, 2) diffusion, 3) electrostatic forces, and 4) adsorption [1, 2]. 1) Mechanical interlocking is the "keying" of the adhesive into the irregularities of the substrate surface [1]. This mechanism is only applicable to substrates with a rough surface. The substrates may be either mechanically or chemically roughened through mechanical abrasion or chemical pretreatments. 2) Diffusion is the movement of a species down a concentration gradient. Adhesion of polymers to each other can occur through mutual diffusion of polymer molecules across the interface [1]. Interdiffusion of polymer chains across the polymer-polymer interface requires that the chain segments of both polymers possess sufficient mobility and are mutually soluble [1]. 3) Electrostatic forces are generated due to the attraction of particles with opposite charges, such as the attraction between a proton and electron. When two surfaces come into contact with each other, there can be an exchange of electrons. This causes the formation of a double layer of electrical charge at the interface [1]. The resulting electrostatic forces bind the two surfaces together. 4) Adsorption is the adhesion of a substance (adsorbate) to a surface (adsorbent). Not to be

confused with absorption, in which the absorbate is dissolved by the absorbent. Adsorption is a surface process, whereas absorption involves the bulk material. Adsorption occurs due to interatomic and intermolecular forces which are established between the atoms and molecules at the surfaces of the substrate and adhesive [1]. When the forces involved are van der Waals forces (secondary bonds), the adsorption process is classified as physisorption (physical adsorption). When the forces involved are ionic, covalent, or metallic bonds (primary bonds), the adsorption process is classified as chemisorption (chemical adsorption) [1]. Figure 1 is a schematic drawing of the different types of atomic and molecular bonds. Adsorption is the main mechanism of adhesion for most substrate-adhesive interfaces [1].

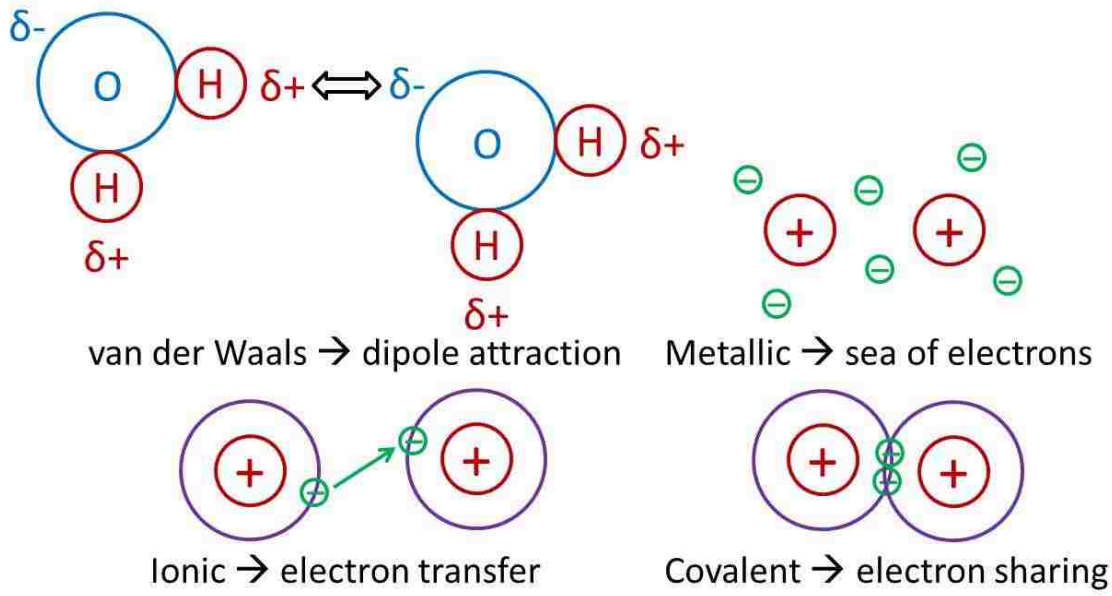

Figure 1. Schematic drawing of the different types of atomic and molecular bonds.

There are many methods for assessing the adhesion of a coating to a substrate by inducing debonding at the substrate-coating interface [2, 3]. Some examples are: peel test, pull test, indentation test, scratch test, blister test, and beam-bending tests (three- and four-point bend test, double cantilevered beam test, wedge test) [3]. Figure 2 depicts three

of the most common adhesion test methods. The choice of which method to use is dependent on many factors, such as the mechanical properties of the coating and substrate, the interface properties, the microstructure of the substrate-coating system, residual stress, coating thickness, and the intended application [2]. I used the indentation method because it is experimentally simple and has no special sample size, geometry, or fixturing requirements. Additionally, the results are directly related to delamination under contact stresses, which is a common failure mechanism in service [4]. I selected the glass-epoxy system because the surface of glass is exceptionally smooth, resulting in a delamination event that is clearly detectable, as will be described in future sections.

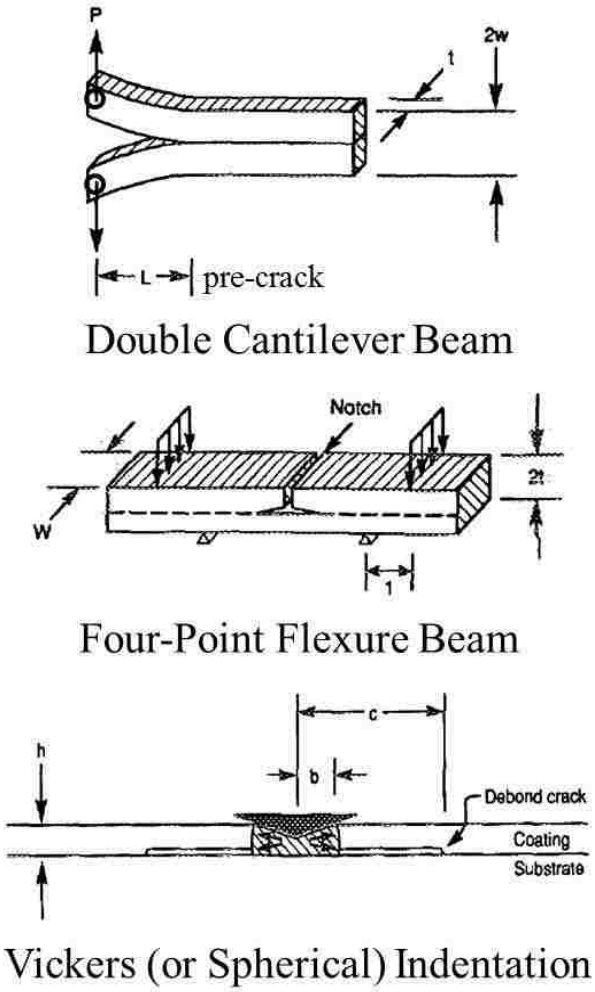

Figure 2. Three common test methods for measuring adhesion. Figure is from Rosenfeld [5].

2. Materials

Soda-lime glass was used for the substrate material. Soda-lime glass is the most common type of glass (used for windowpanes and glass containers) and is relatively inexpensive. It is called soda-lime glass due its composition, which contains sodium carbonate (soda) and calcium oxide (lime). Soda-lime glass samples measuring 3 x 3 x 0.25 inch were purchased. I cut these samples into four pieces, so that my samples were 1.5 x 1.5 x 0.25 inch. I tested glass samples that had been treated/processed differently. I tested smooth glass (surface roughness ~0.03 microns), rough glass (surface roughness ~0.3 microns), stressed glass (tempered), and dirty glass (some without cleaning prior to coating and some were sprayed with a mold release before coating). The glass samples were cleaned (except the dirty glass) and coated with thin epoxy layers.

Epoxy is the most common type of thermoset polymer. Thermosets cannot be reformed once they solidify. Epoxy is a strong adhesive that is used to bond materials together or to cover the surface of a material for protection. An epoxy is formed by mixing two compounds that are in a liquid state at room temperature to form an epoxy resin, which solidifies into a cross-linked lattice upon curing. I used an epoxy that was a mixture of diglycidyl ether of bisphenol A (Epon 828) cured with diethanolamine (DEA) at a ratio of 100 to 12 parts by weight. The abbreviated name for this epoxy is Epon 828/DEA. Two different thicknesses of epoxy coatings (150 and 250 microns) were used.

3. Experimental Method

Indentation experiments were performed using an Instron 5565 Universal Testing Machine (UTM) with an environmental chamber at Sandia National Laboratories in Albuquerque, NM. A stainless steel (SS) spherical indenter (1/16th inch diameter) was used, unless otherwise noted. The indenter assembly was attached to a load cell bolted to the bottom of the UTM crosshead. A motor moved the crosshead at a rate of 0.05 mm/min. An acoustic sensor was mounted in the environmental chamber to capture any sounds associated with delamination. Indenter load, displacement, and acoustic signal were recorded every 2 ms. Figure 3 shows the experimental setup.

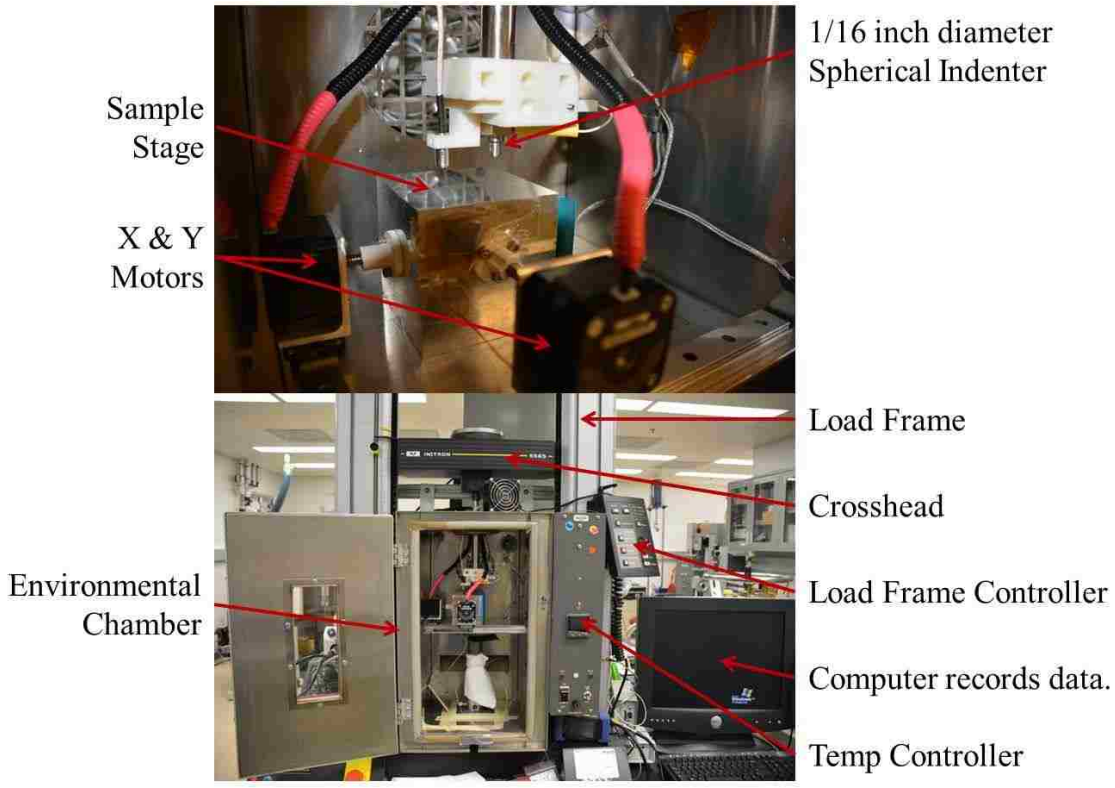

Figure 3. Experimental setup of the Instron 5565 UTM with an environmental chamber.

During the indentation experiments, the coated surface of the sample is loaded with a spherical indenter (Figure 4). The coating is deformed and displaced laterally by

the indenter. This lateral displacement produces a shear stress across the glass-epoxy interface and results in delamination of the epoxy coating from the glass substrate at sufficiently high loads [4, 6]. Indentation experiments were conducted in an environmental chamber at -55°C (cooled with liquid Nitrogen) to induce a residual tensile stress in the epoxy coating due to a thermal expansion mismatch between the glass and epoxy. The coefficient of thermal expansion for epoxy is about 10 times greater than glass. This residual stress adds to the shear stress generated by the indenter and enables delamination at lower indenter loads. At higher loads, the indenter will penetrate through the epoxy coating and impact the glass substrate, thus invalidating the experiment. Figure 5 shows the results of indentation tests performed on alumina substrate-epoxy coated samples at different temperatures (experiments and imaging done by Cory Gibson, Sandia National Laboratories, NM). At the center of the images is deformation from the indenter. Three of the tests done at cold temperatures have clear delaminations. The optimal temperature for future indentation tests was chosen to be -55°C.

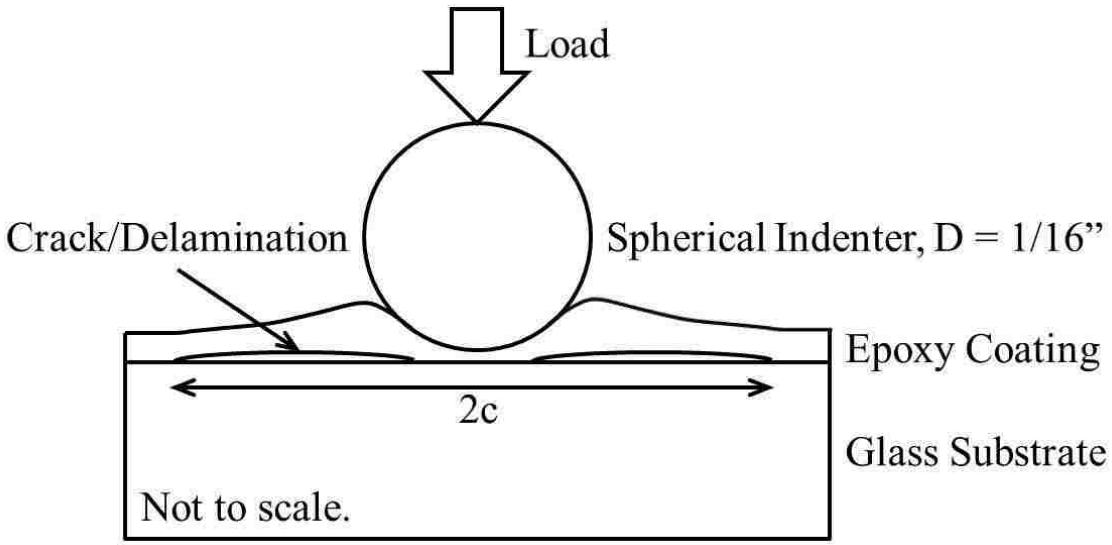

Figure 4. Schematic drawing of spherical indentation.

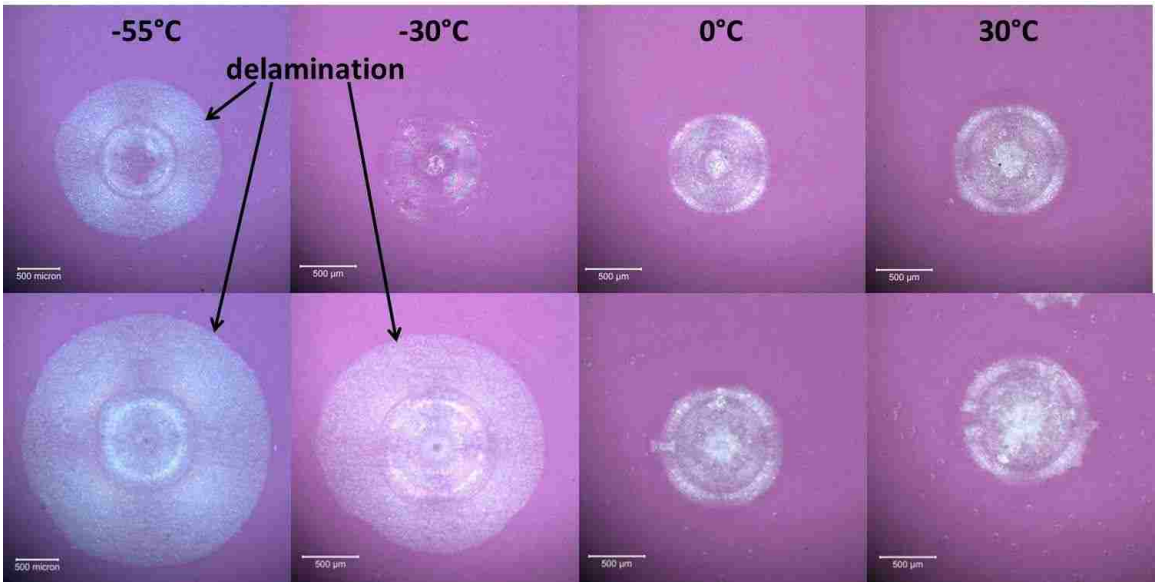

Figure 5. Results of indentation tests performed on alumina substrate-epoxy coated samples done at a range of temperatures. The load for the top row was 50 kg and the bottom row was 80 kg. It is clear that lowering the temperature promotes delamination. The indentation tests and imaging were performed by Cory Gibson at Sandia National Laboratories in NM.

Tang et al. [7] demonstrated that a multilayered composite consisting of alternating soft (Al) and hard (SiC) nanolayers can experience delamination at the silicon substrate interface and also between nanolayers. They used the finite element method to model the stresses due to nanoindentation. Figure 6 shows the results of their modeling. Underneath the indenter is a zone of compression and adjacent to that is a region of tension. The tension enables delamination to occur at the interface and also between nanolayers (Figure 7). Thus, the dominant driving force for delamination of nanolayers is a vertical tensile stress perpendicular to the interface, while thicker (μm-scale) coatings delaminate due to in-plane shear stress at the substrate-coating interface.

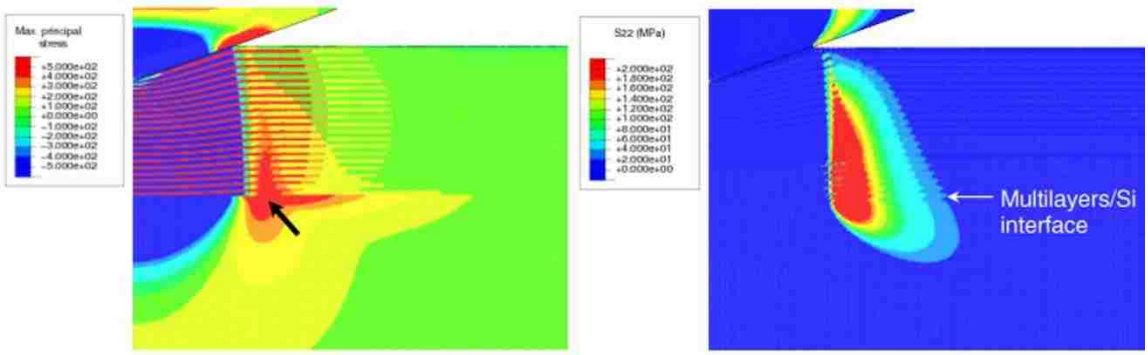

Figure 6. Contours of maximum principal stress (left) and vertical tensile stress (right) near the indentation site. Indentation depth is 500 nm. Figure is from Tang et al. [7].

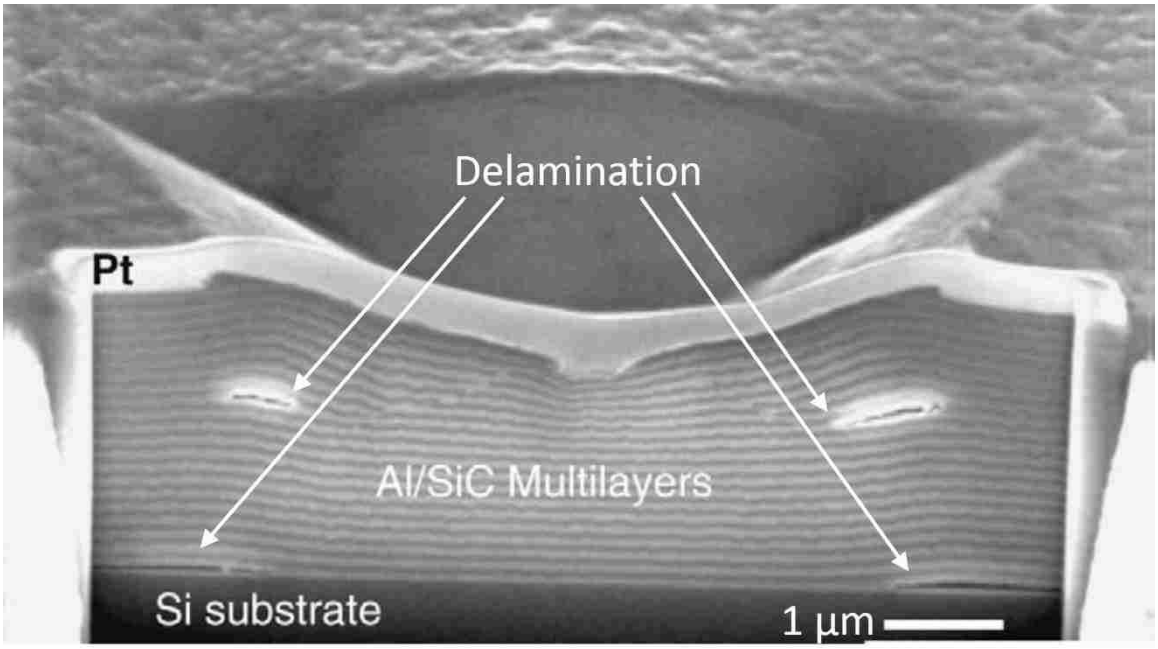

Figure 7. Cross-section showing delamination at the substrate-multilayered composite interface and also between two nanolayers. Figure is from Tang et al. [7].

Figure 8 is a load-displacement curve for one indentation. When delamination occurs, there is a small and sudden drop in load. The delamination load is the maximum load before the drop. The sample is then unloaded and moved to perform the next indent. The acoustic signal has a spike ("pop") that corresponds with the drop in load at delamination. Figure 9 is a cross-section of an indentation site that shows delamination of the epoxy coating from the glass substrate, similar to the drawing in Figure 4. During

polishing of the sample, some polishing material entered into the delaminated region, making the delamination more noticeable. Figure 10 shows top views of an indent with delamination of the epoxy coating from the glass substrate. The size of the delamination is most easily measured using reflected light, due to the delaminated region being at a slightly different height than the surrounding epoxy. The transmitted-light image shows the pileup of epoxy around the contact area of the indenter. For comparison, Figure 11 shows images of an indent that was performed at room temperature and 50 kg, illustrating cracking in the glass (dark regions at the center) that occurred when the indenter penetrated through the epoxy coating and impacted the glass surface. There was no delamination event (no drop in load or "pop") and there was a large amount of epoxy pileup around the indenter contact area. For these reasons, I needed to perform the experiments at cold temperature to enable delamination at lower indenter loads.

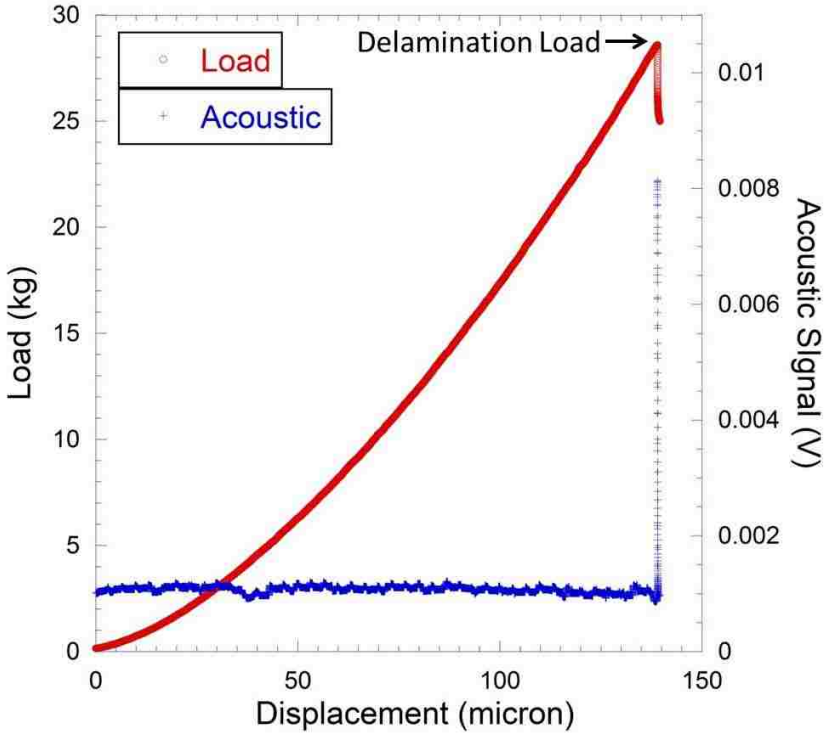

Figure 8. Load-displacement curve for a typical indent. A spike in the acoustic signal corresponds with the drop in load at delamination.

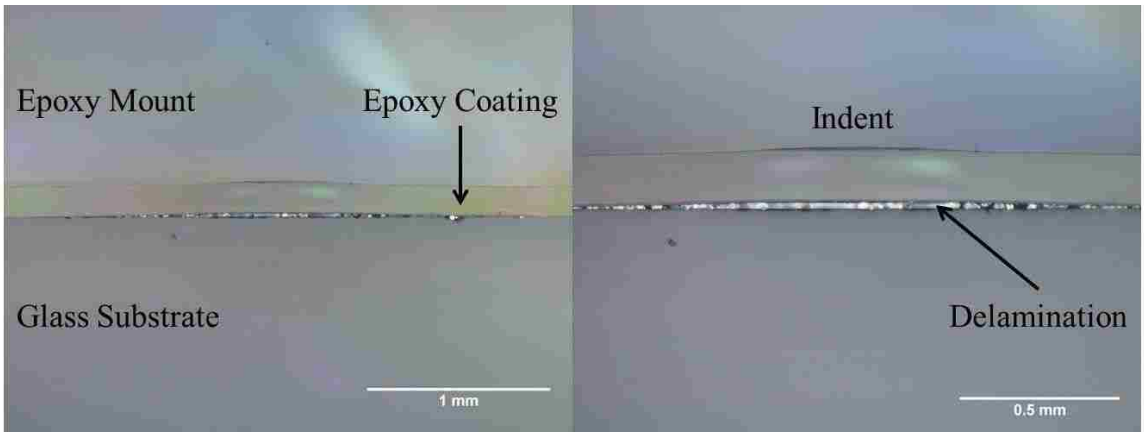

Figure 9. Cross-section of an indentation site showing delamination of the epoxy coating from the glass substrate. The image on the right is a higher magnification.

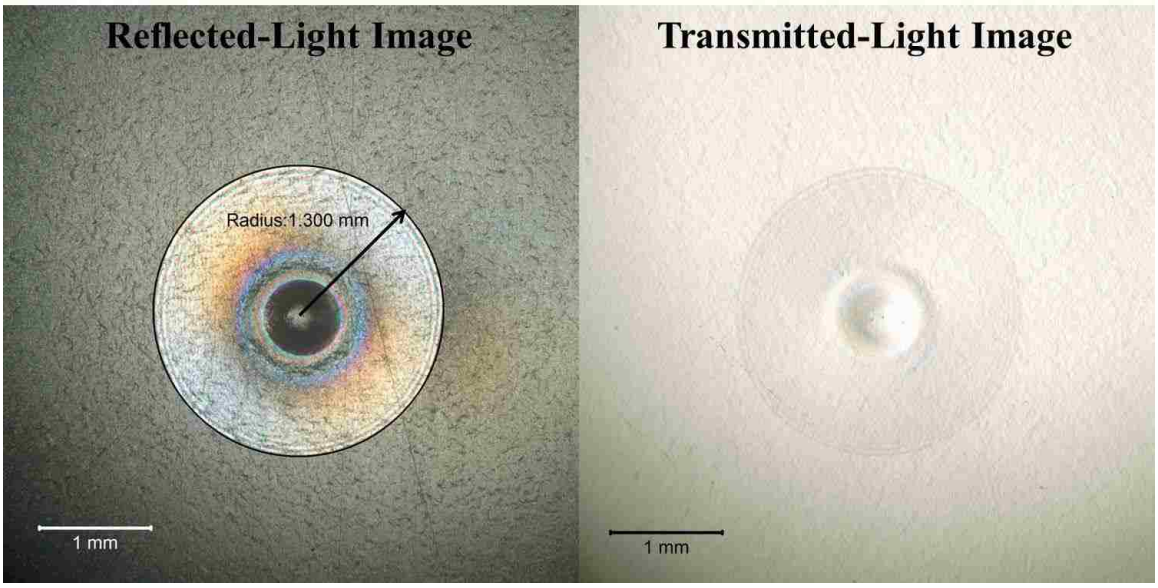

Figure 10. Top views of an indentation site showing delamination of the epoxy coating from the glass substrate.

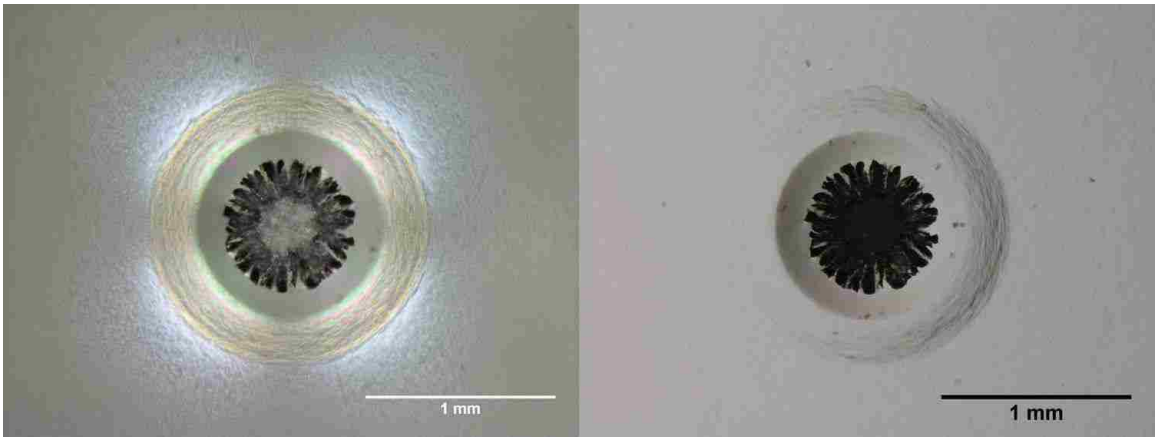

Figure 11. Images taken in cross-polarized light (left) and transmitted light (right) of an indent performed at room temperature and 50 kg, illustrating the damage to the glass when the indenter impacted the glass substrate. The transmitted light image shows a large amount of epoxy pileup around the indenter contact area.

To determine if the spacing between indents had a significant effect on the delamination sizes, I performed 9 indents that were about 10 mm apart on one sample and 9 indents that were about 5 mm apart on another sample (Figure 12). There was no difference in the delamination sizes. Therefore, I used the closer spacing in my experiments so that more indents could fit on each sample. However, movement of the sample stage is controlled by a toggle switch and is not able to be precisely controlled.

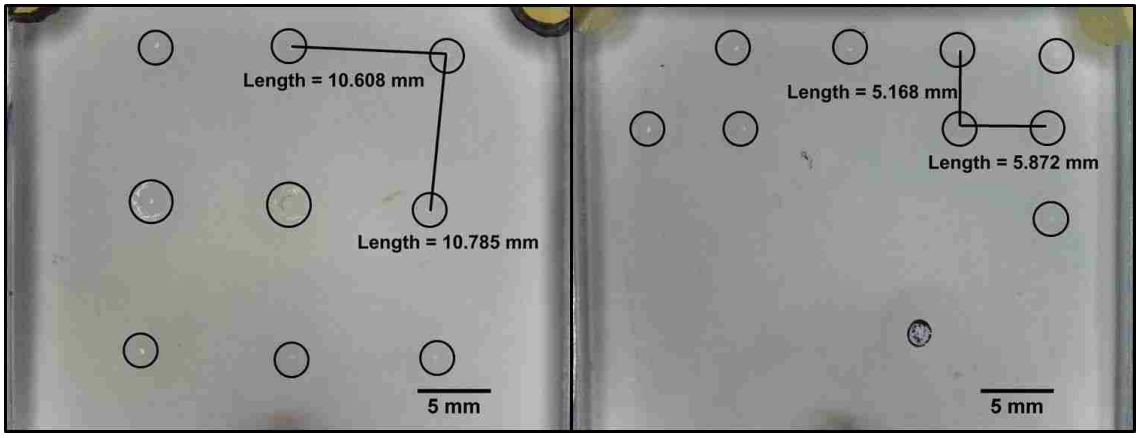

Figure 12. Delamination size (circled) as a function of indent spacing. The sizes are the same whether the indents are about 10 mm apart or 5 mm apart.

I performed some indentations on a sample with a 250 micron epoxy coating at different crosshead rates to see if indenter speed had an effect on delamination. Figure 13 is a boxplot showing the results. The boxes show the ranges of values, the horizontal lines through the boxes are the median values, and the average values are labeled. I performed 10 indents using a rate of 0.05 mm/min and 3 indents at each of the other rates. The average values do not appear to be significantly different over the range of crosshead rates tested. It appears that indenter speed does not have a significant effect on delamination. All other experiments were done using a rate of 0.05 mm/min because that is the standard rate used by the Materials Mechanics and Tribology group at Sandia National Laboratories, NM.

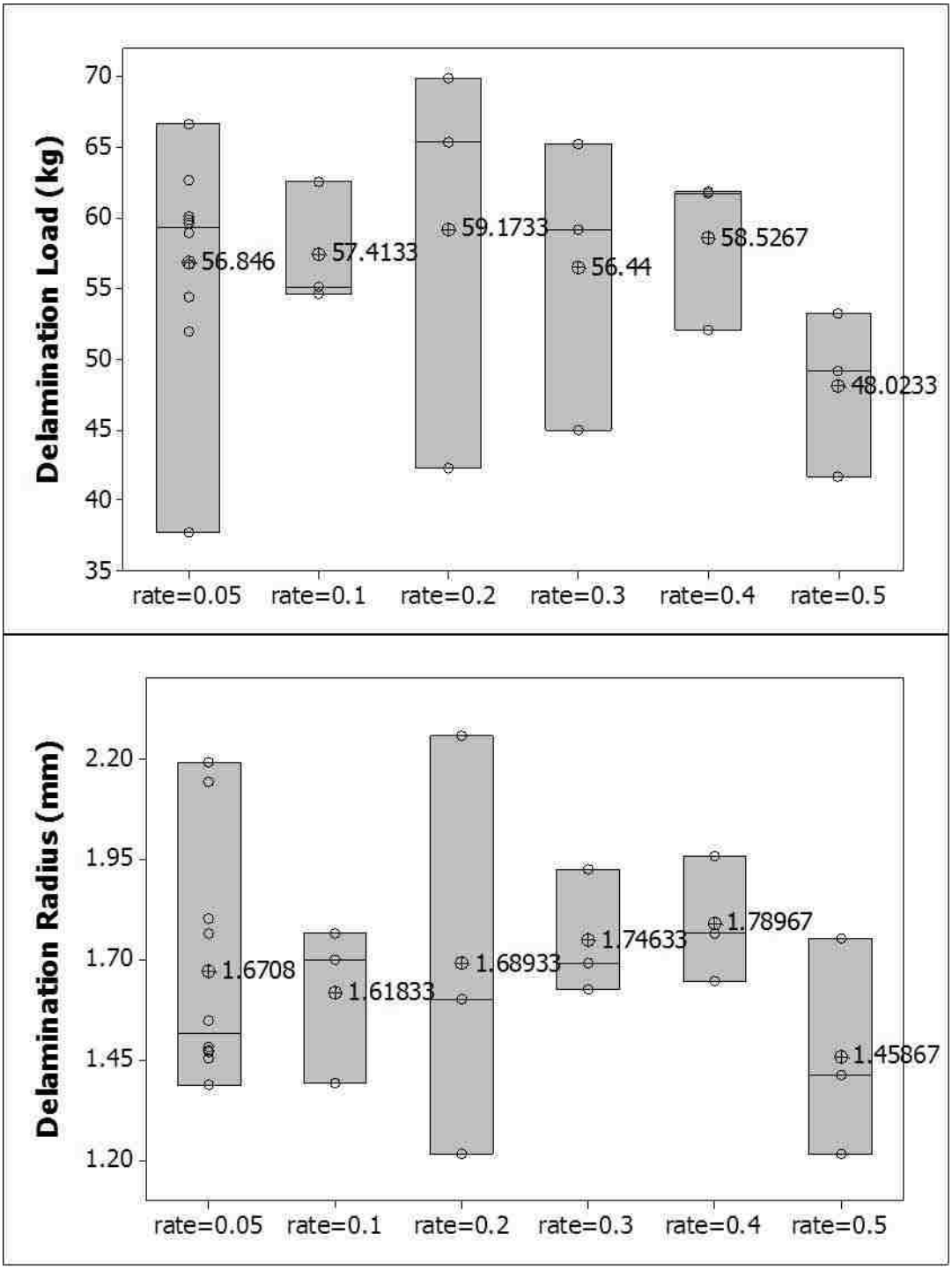

Figure 13. Ranges of delamination loads and radii for different indenter rates. The average values for each indenter rate are labeled.

4. Experimental Results

4.1. Cracking in the Glass Substrate

An unforeseen problem that I encountered was cracking in the glass substrate, even though the indenter did not penetrate through the epoxy coating and impact the glass surface. The cracking appears to be partial cone-cracking. Cone cracking is initiated by a surface defect that grows into a ring crack and then penetrates down into the glass substrate at an angle in the shape of a cone [8]. Figure 14 is a schematic drawing depicting the formation of a cone crack. Underneath the indenter is a compression zone due to the applied load. Surrounding the compression zone is a region of tension. The tension at the glass surface enables the surface defect to grow into a ring crack. Once a critical load is reached, the ring crack grows into a cone crack. The cracking in the glass is not load dependent. It is just as likely to occur at 30 kg as 80 kg. The cracking occurs when the indentation takes place near a surface defect in the glass. Figure 15 shows top views of an indentation site taken in transmitted light and using a ring light (the light hits the surface at an angle). Figure 16 is a cross-section of the same indent, showing cracking in the glass substrate. The cracked area appears black because the light is reflected away at a different angle by the crack.

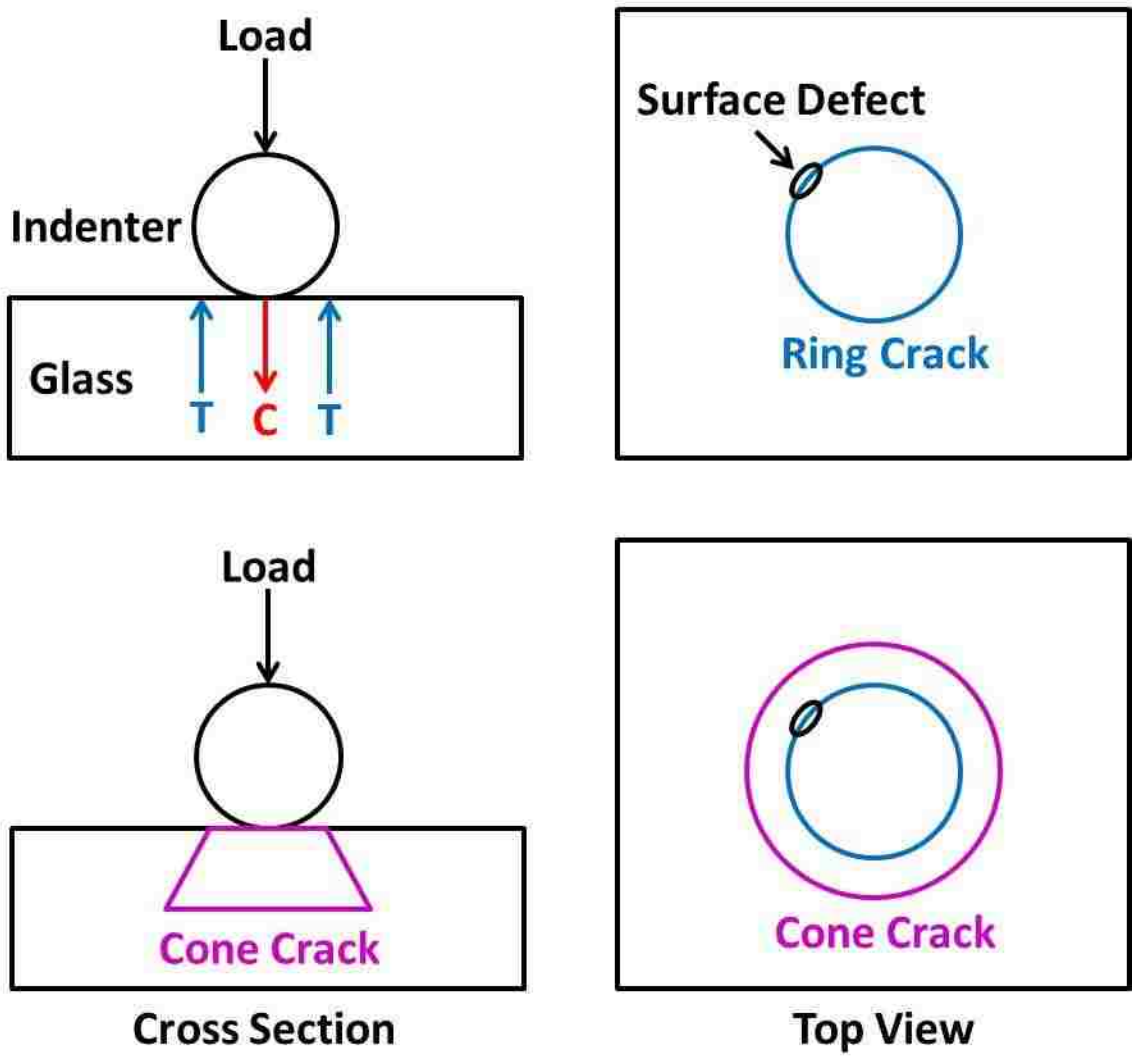

Figure 14. Schematic drawing depicting the formation of a cone crack. A surface defect grows into a ring crack then penetrates down into the glass substrate, forming a cone crack. C = compression, T = tension.

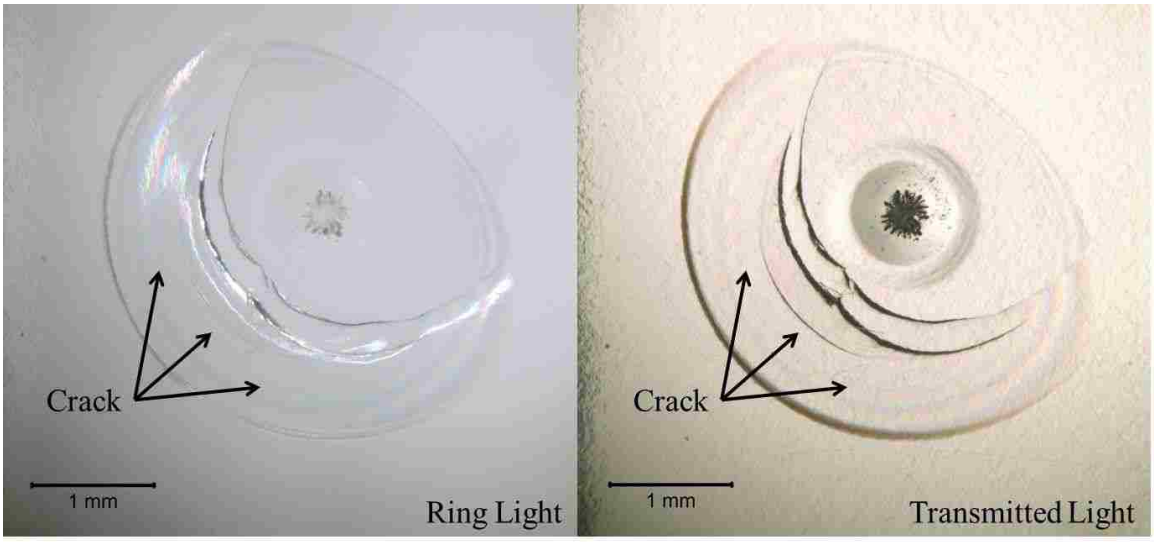

Figure 15. Top views of an indentation site with cracking in the glass substrate.

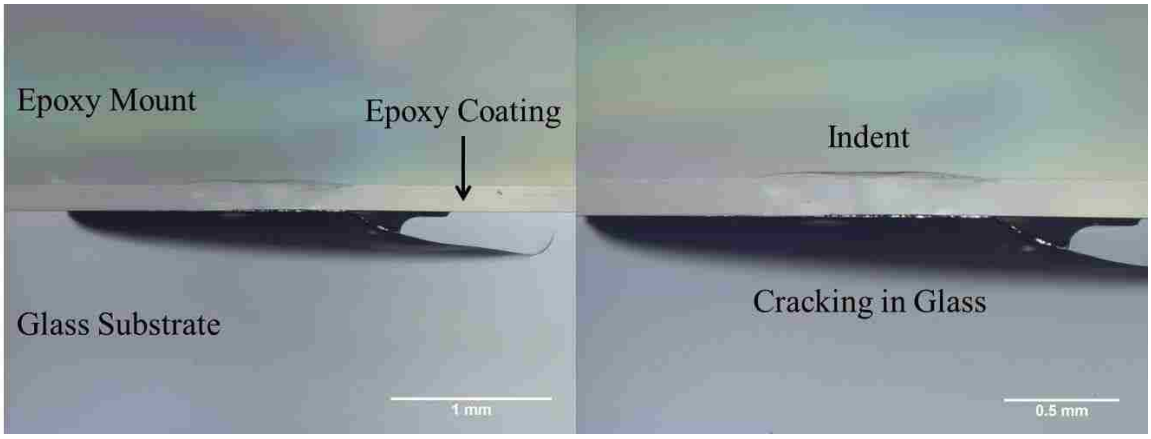

Figure 16. Cross-section of an indentation site with cracking in the glass substrate. The image on the right is a higher magnification.

4.2. Smooth Glass with Epoxy Coating

I performed 20 indents on smooth glass samples with 150 micron epoxy coatings and 9 of those indentations had cracking in the glass substrate. I also performed 20 indents on smooth glass samples with 250 micron epoxy coatings and 5 of them had glass cracking. Table 1 is a summary of the delamination data for both the 150 and 250 micron epoxy coatings. When glass cracking occurs, the delamination sizes and loads tend to be larger, thus increasing variability in the data. A comparison of the delamination data when the indents with cracked glass were excluded or included is shown in Figure 17. It is clear there is more scatter in the data when the indents with cracked glass are included. It is also evident that a higher load is required to delaminate the thicker coating and that delamination size generally increases with load. The higher load is required because there is a greater distance for the load to be transferred to the interface. The delamination size increases with load due to a larger release of energy when cracking/debonding occurs.

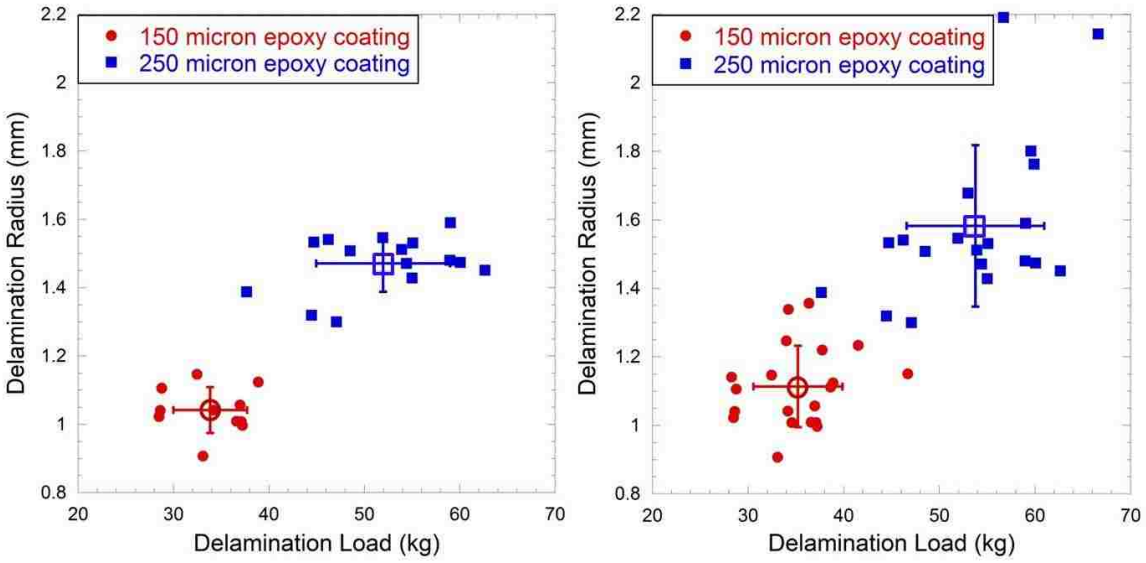

Figure 17. Comparison of delamination data when the indents with glass cracking are excluded (left) and included (right). The average values for each group are also plotted with error bars denoting the standard deviations.

Table 1. Summary of the delamination data for smooth glass with epoxy coatings.

150 micron epoxy coating	Excluding Cracked Indents	Including Cracked Indents
Average Delamination Load (kg)	33.8	35.2
Standard Deviation Load (kg)	3.9	4.7
Avg. Delamination Radius (mm)	1.04	1.11
Standard Deviation Radius (mm)	0.07	0.12
250 micron epoxy coating		
Average Delamination Load (kg)	52.0	53.8
Standard Deviation Load (kg)	7.0	7.2
Avg. Delamination Radius (mm)	1.47	1.58
Standard Deviation Radius (mm)	0.08	0.24

To further investigate the trend of delamination size increasing with load, I did some indentations at loads higher than the delamination load. I did 5 indents each at 50, 60, 70, and 80 kg on the 150 micron epoxy coating. I did the same for the 250 micron epoxy coating except for 50 kg, since that is the delamination load for the thicker coating. Figure 18 is a plot of the high-load data, excluding and including the data when the indents had glass cracking. The average delamination values with error bars denoting the standard deviations are also plotted. The best-fit lines clearly demonstrate that the delamination size continues to grow as the load is increased past the delamination load. It is also evident that the delamination sizes at a given load are larger for the 250 micron epoxy coating than the 150 micron epoxy coating. This is due to the higher strain energy associated with the thicker coating, which is also why the delamination size increases at a faster rate (steeper slope) for the thicker coating.

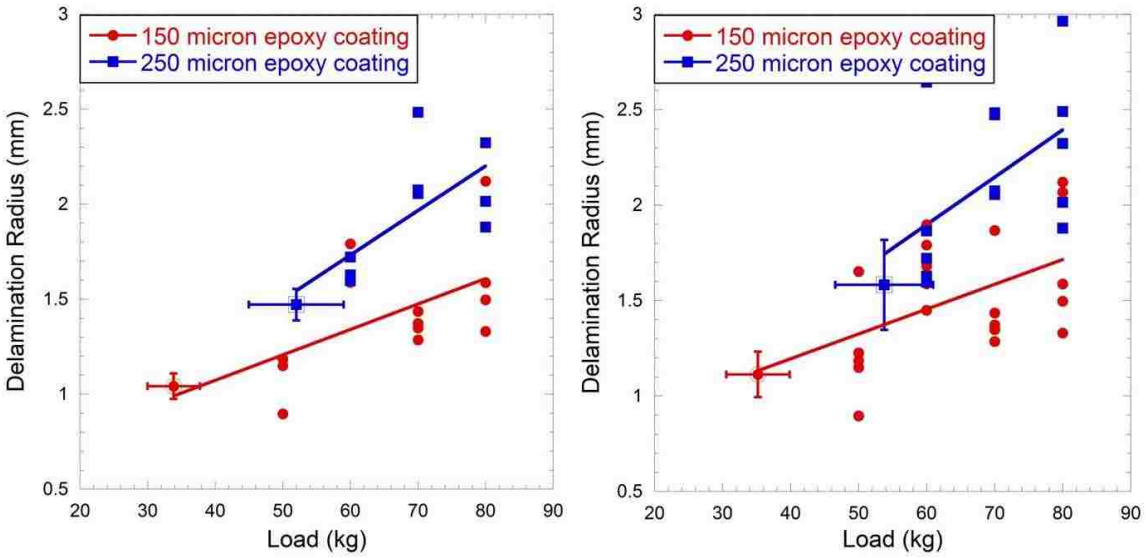

Figure 18. Delamination size increases as the load is increased past the delamination load. The plot on the left has indents with glass cracking excluded and the plot on the right has them included. The average delamination values with error bars are also plotted.

I also performed 12 indents on a smooth glass sample with 150 micron epoxy coating using a Vickers indenter. One indent had cracking and was excluded from analysis. A Vickers indenter has a 4-sided pyramidal diamond tip. Figure 19 shows top views of an indentation made with a Vickers indenter in reflected and transmitted light. The average delamination load with the Vickers indenter was 27.8 ± 2.6 kg, compared to 33.8 ± 3.9 kg with the spherical indenter. The average delamination radius with the Vickers indenter was 0.88 ± 0.07 mm, compared to 1.04 ± 0.07 mm with the spherical indenter. Delamination occurs at a slightly lower load using the Vickers indenter, with a corresponding smaller delamination radius, than the spherical indenter. This is because the Vickers indenter tip is sharp and therefore it is easier to penetrate through the epoxy. In fact, for half of the Vickers indents, the indenter penetrated through the epoxy coating and into the glass substrate. Figure 20 is a plot showing the indenter displacement (penetration depth) for each Vickers indent. The coating thickness for this particular

sample was 160 microns, therefore displacements greater than that indicate the indenter penetrated into the glass substrate. Due to this problem, I used a spherical indenter for all other indentation experiments. Using a spherical indenter, the penetration depth was less than three-quarters of the coating thickness for all indentation tests.

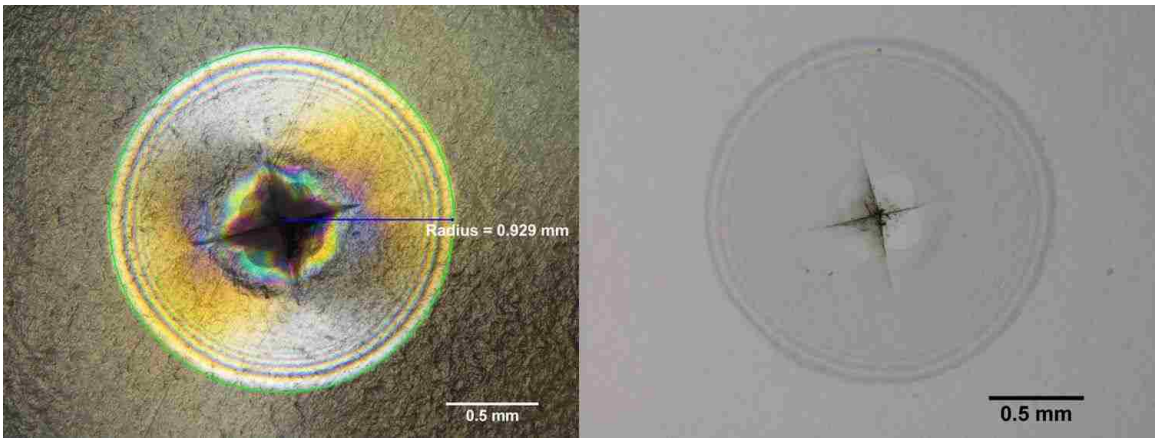

Figure 19. Images taken in reflected light (left) and transmitted light (right) of a Vickers indent with delamination of the epoxy coating.

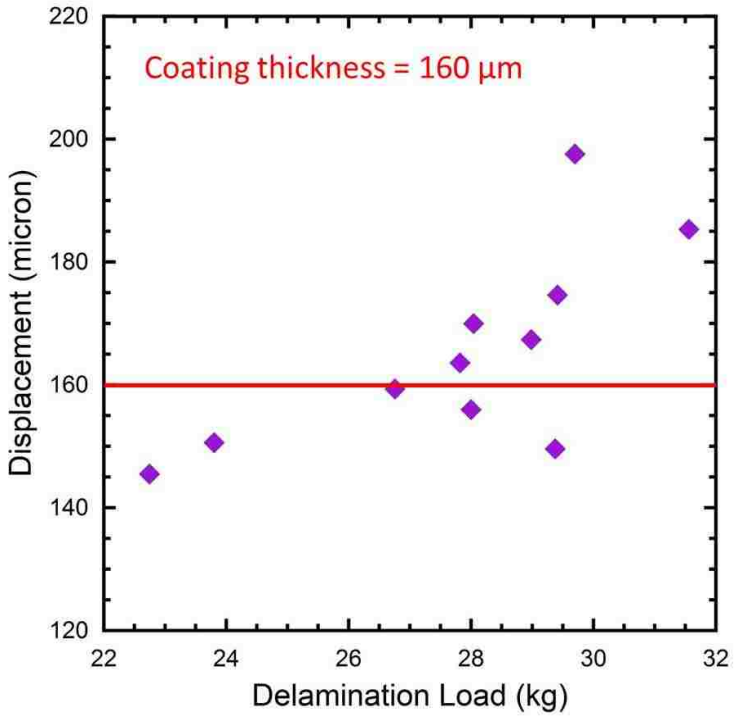

Figure 20. Plot of the Vickers indentation data showing that 6 of the 11 indents penetrated through the epoxy coating and into the glass substrate.

4.3. Rough Glass with Epoxy Coating

I performed 10 indents on a glass sample that had a surface roughness of 0.3 microns (10 times rougher than the smooth glass) and a 150 micron epoxy coating. Glass cracking occurred in all of the indentations because the abraded glass surface is covered with defects. The average delamination load was 45 ± 6 kg, about 10 kg higher than the smooth glass with 150 micron epoxy coating. Figure 21 shows top views of an indentation site taken in transmitted light and using a ring light. The average delamination radius is 0.88 ± 0.13 mm for the rough glass, compared to 1.04 ± 0.07 mm for the smooth glass. The delaminated area has an irregular shape and does not extend out to the edges of the cracking in the glass substrate, as it does with the smooth glass. Figure 22 is a cross-section of the same indent, showing that the size of the central delaminated region matches with the size measured on the transmitted light image (diameter about 1.7 mm). The rough glass surface has better adhesion due to mechanical interlocking and increased surface area, thus requiring a higher load to delaminate with a smaller delaminated region. However, cracking in the brittle substrate always occurs due to numerous surface defects.

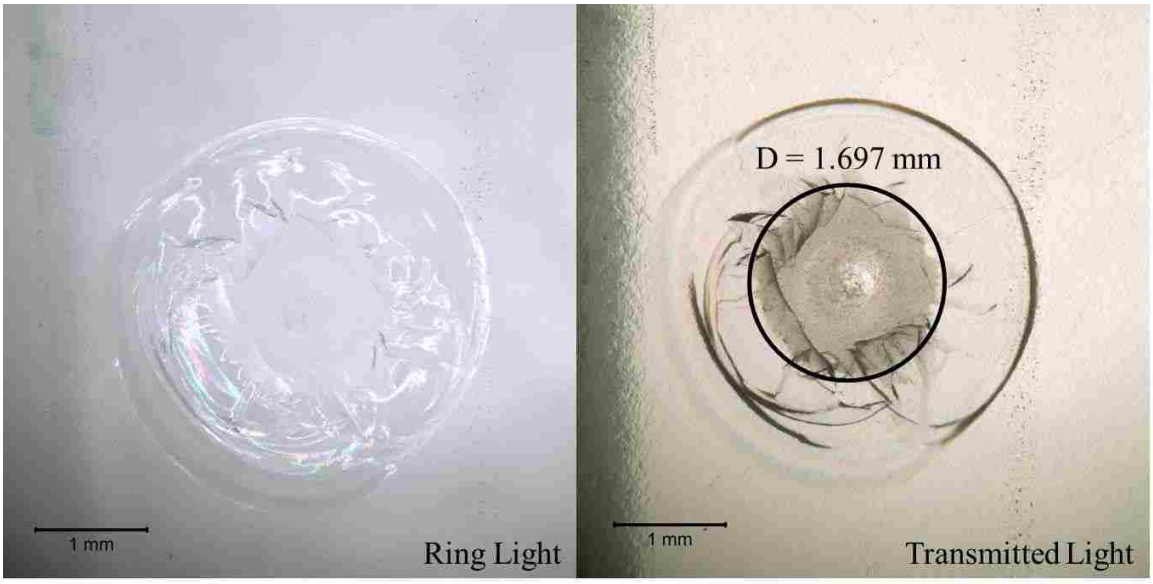

Figure 21. Top views of an indentation site on a rough glass sample with epoxy coating. The circle drawn on the transmitted light image denotes the delaminated region (dark area).

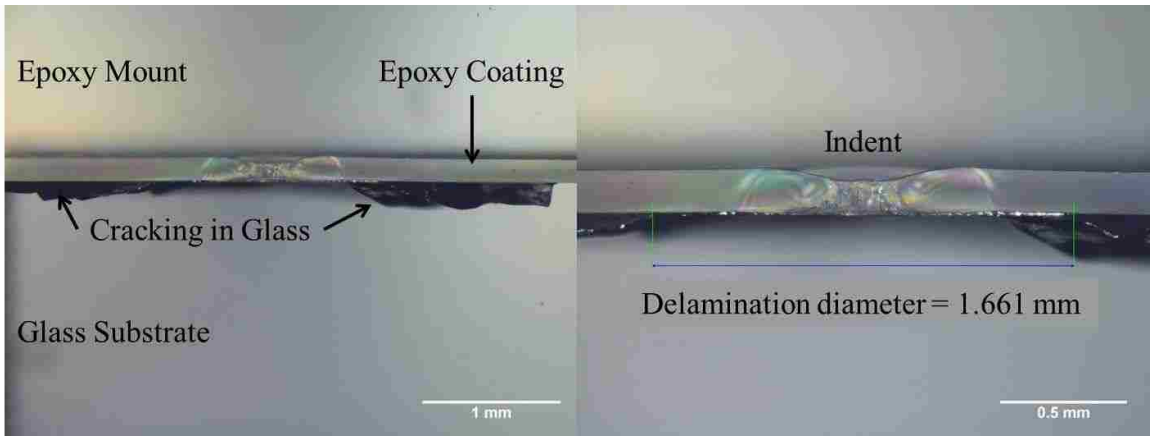

Figure 22. Cross-section of an indentation site on a rough glass sample showing cracking in the glass substrate and the central delaminated region. The image on the right is a higher magnification.

4.4. Dirty Glass with Epoxy Coating

Two smooth glass samples (one for each coating thickness) were handled and not cleaned prior to epoxy coating. I performed 9 indents on the 150 micron epoxy coating and 10 indents on the 250 micron epoxy coating (2 were excluded due to glass cracking). Another two smooth glass samples were sprayed with a mold release before coating, which contaminated the glass surface. I performed 9 indents on the 150 micron epoxy coating (2 were excluded due to glass cracking) and 10 indents on the 250 micron epoxy coating (2 were excluded due to glass cracking). A summary of the delamination results is displayed in Table 2 and plotted in Figure 23. It is clear that the samples with dirty glass and glass sprayed with mold release delaminate at lower loads than the clean glass samples (from section 4.2.). The surface contaminates interfere with bonding at the interface, thus making delamination easier (lower adhesion). It is also evident that the samples with mold release have a larger amount of variability (much larger error bars).

Table 2. Summary of the delamination data for dirty glass with epoxy coatings.

150 micron epoxy coating	Glass that was handled	Glass sprayed w/ mold release
Average Delamination Load (kg)	29.2	27.6
Standard Deviation Load (kg)	3.9	6.7
Avg. Delamination Radius (mm)	0.92	1.04
Standard Deviation Radius (mm)	0.09	0.27
250 micron epoxy coating		
Average Delamination Load (kg)	37.7	38.6
Standard Deviation Load (kg)	3.26	10.05
Avg. Delamination Radius (mm)	1.35	1.47
Standard Deviation Radius (mm)	0.07	0.44

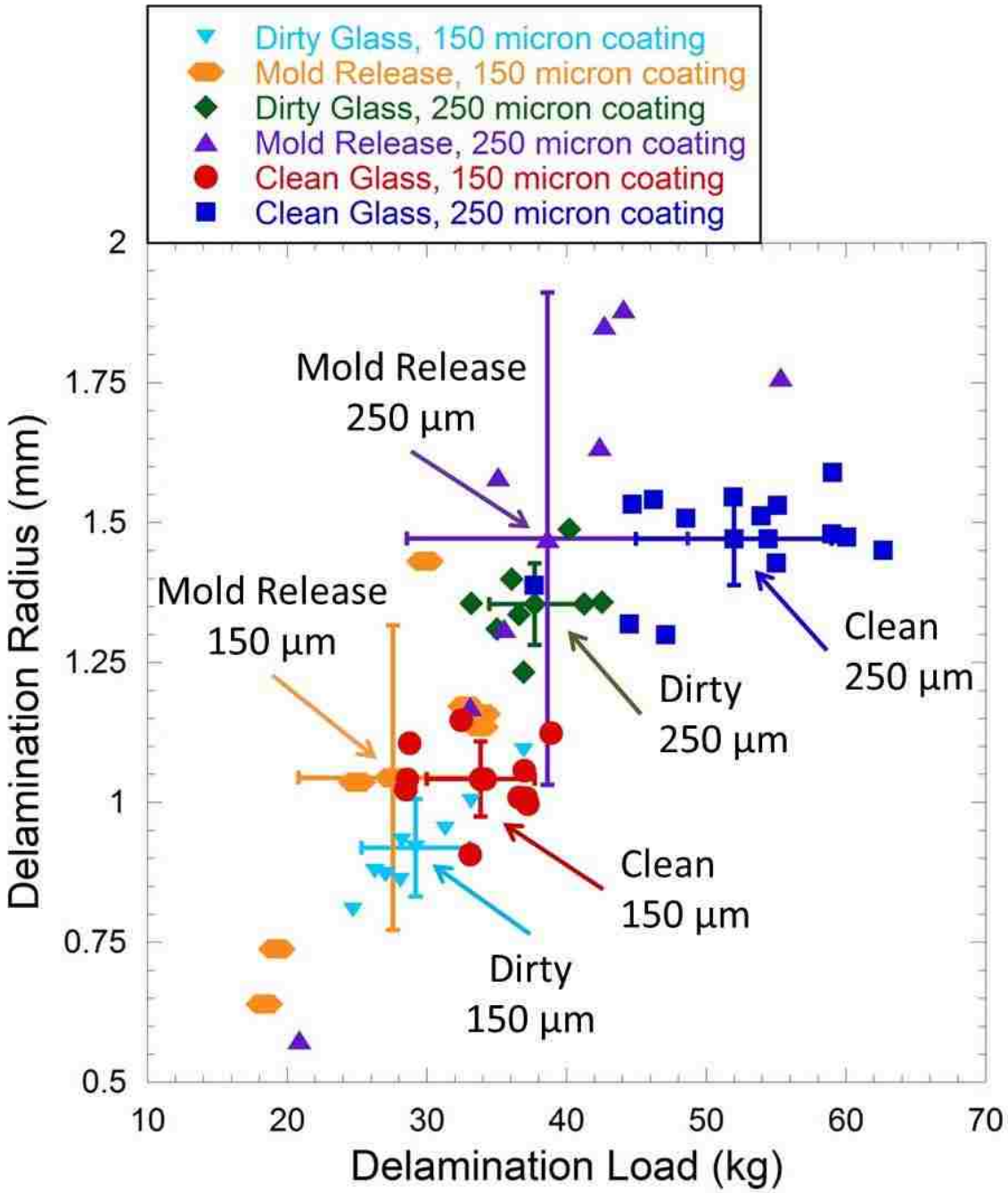

Figure 23. Delamination results for glass samples that were handled (dirty) and sprayed with a mold release. The clean glass results are also plotted for comparison. The average values for each group with error bars denoting the standard deviations are also plotted.

4.5. Stressed Glass with Epoxy Coating

I tested two glass samples (one for each coating thickness) that had been tempered to see if the residual compressive stress present at the glass surface would interact with the shear stress imparted by the indenter during loading and influence the delamination loads. Tempered glass is glass that has been processed by thermal or chemical treatments to increase its strength. Thermal treatments involve heating and quenching the glass, while chemical treatments involve ion exchange with larger ions replacing smaller ions at the glass surface. These treatments cause the outer surface of the glass to be in compression, balanced by tension in the inner core. These stresses cause the glass to break into small chunks rather than jagged shards when broken. The compressive stress at the surface tends to close any defects, thus increasing the strength of the glass. For these reasons, tempered glass is used as safety glass.

I tested one stressed (tempered) glass sample with a 150 micron epoxy coating and one with a 250 micron epoxy coating. These glass samples were circular (not square, like the other samples) with a diameter of 1.5 inch. I also had two non-stressed circular glass samples coated with 150 and 250 micron epoxy coatings so that the size and geometry of the samples would be the same for comparison of results. I performed 10 indents on each of the four samples (two stressed and two non-stressed). The stressed glass with 150 micron epoxy coating had one indent with glass cracking and the stressed glass with 250 micron epoxy coating had 3 indents with glass cracking. The non-stressed glass with 150 micron epoxy coating had 4 indents with glass cracking and the non-stressed glass with 250 micron epoxy coating had one indent with glass cracking. The indents with cracking in the glass substrates were excluded from analysis. Figure 24 is a

plot of the results and Table 3 is a summary of the delamination data. On average, the stressed glass samples delaminated at lower loads with smaller delamination sizes. This suggests that the residual compressive stress at the glass surface aids in delamination of the epoxy coating.

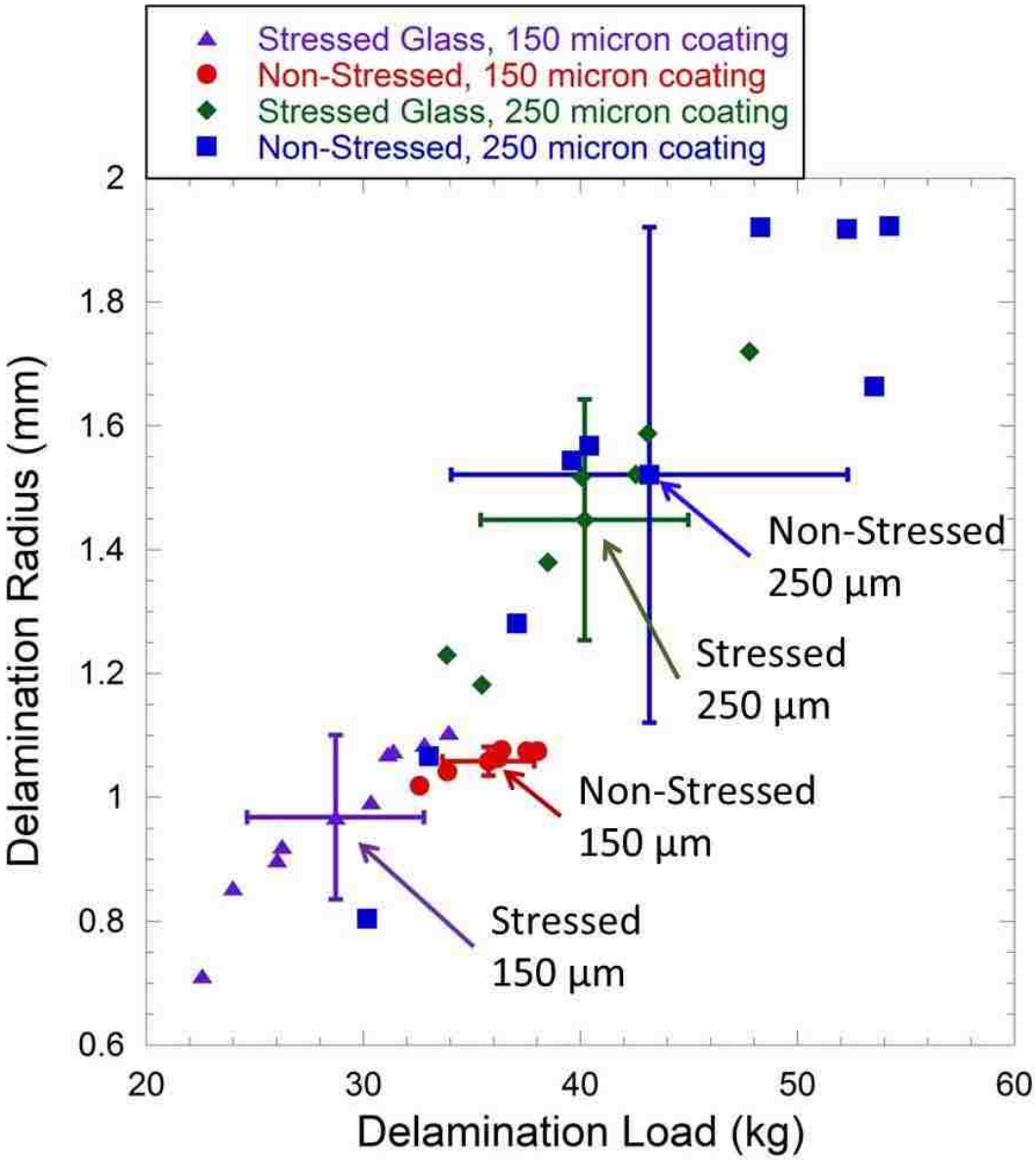

Figure 24. Delamination results for stressed (tempered) glass versus non-stressed glass. The average values for each group with error bars denoting the standard deviations are also plotted.

Table 3. Summary of the delamination data for stressed (tempered) glass versus non-stressed glass.

150 micron epoxy coating	Stressed Glass	Non-Stressed Glass
Average Delamination Load (kg)	28.7	35.8
Standard Deviation Load (kg)	4.1	2.1
Avg. Delamination Radius (mm)	0.97	1.06
Standard Deviation Radius (mm)	0.13	0.02
250 micron epoxy coating		
Average Delamination Load (kg)	40.2	43.2
Standard Deviation Load (kg)	4.8	9.1
Avg. Delamination Radius (mm)	1.45	1.52
Standard Deviation Radius (mm)	0.19	0.40

4.6. Calculation of the Epoxy Properties

In order to calculate the interfacial fracture energy of the glass-epoxy system, the hardness and elastic modulus of the epoxy must be known. I did my experiments at -55°C to promote delamination at lower loads. Therefore, the hardness and elastic modulus at that temperature are required. I performed 8 spherical indentations on a bulk epoxy sample (thickness about 0.5 inch) and collected both loading and unloading data. The sample was unloaded at the same rate as it was loaded (0.05 mm/min). For 4 of the indentations, I held the indenter at the maximum load for 10 seconds before unloading and the other 4 indentations were held at the maximum displacement for 10 seconds before unloading. The 10 second hold is to allow the epoxy time to recover from viscoelastic effects (both viscous and elastic characteristics during deformation) before unloading. The maximum load was 50 kg and the maximum displacement was the displacement at 50 kg. Figure 25 shows an example of each type of hold. The Instron machine performed better at holding the load constant than holding the displacement constant (there was a little drift in the displacement hold).

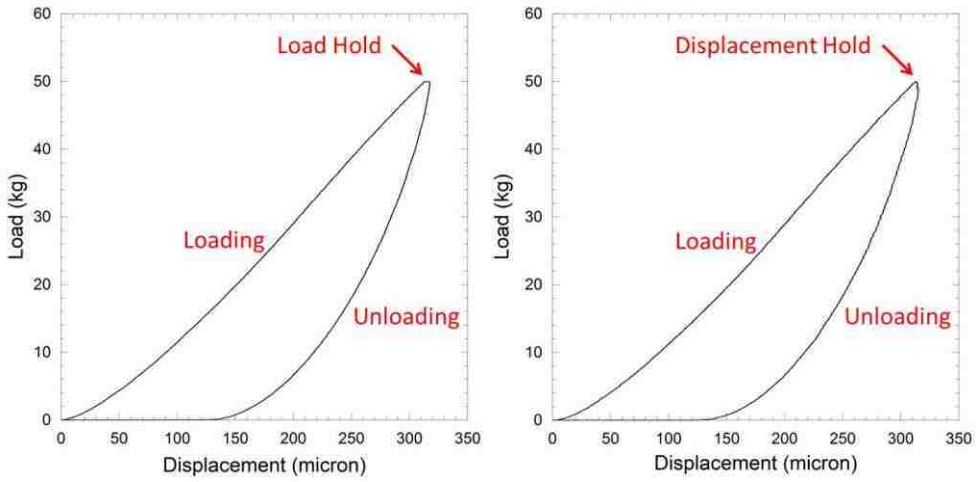

Figure 25. Comparison of loading-unloading curves for indentations on a bulk epoxy sample that had a load hold versus a displacement hold.

The Oliver and Pharr method [9, 10, 11] fits the upper half of the unloading curve (after the hold) with the following equation:

$$P = A\left(h - h_f\right)^m \tag{1}$$

where P is the indenter load (y variable), h is the displacement into the surface (x variable), and A, m, and h_f are fitting constants. Once the fitting constants are obtained by fitting the upper half of the unloading curve with Equation 1, the hardness and elastic modulus can be calculated using the following equations [9, 10, 11]:

$$S = mA(h - h_f)^{m-1} \tag{2}$$

$$h_c = h - 0.75(P/S) \tag{3}$$

$$A_c = 2\pi R h_c \tag{4}$$

$$H = P/A_c \tag{5}$$

$$E_r = \frac{S\sqrt{\pi}}{2\sqrt{A_c}} \tag{6}$$

$$E = (1 - \nu^2)\left[\frac{1}{E_r} - \frac{(1-\nu_i^2)}{E_i}\right]^{-1} \tag{7}$$

where S is the unloading stiffness, h_c is the contact depth, A_c is the contact area, R is the indenter radius, H is the epoxy hardness, E_r is the epoxy reduced elastic modulus, E is the epoxy elastic modulus, ν is the epoxy Poisson's ratio, E_i is the indenter elastic modulus, and ν_i is the indenter Poisson's ratio. These equations are tailored for a spherical indenter. I used a stainless steel indenter with R = 794 μm, E_i = 200 GPa, and ν_i = 0.27. Poisson's ratio for the epoxy is 0.4. Figure 26 shows the fit of Equation 1 to the unloading curves plotted in Figure 25 with the fitting constants displayed. The small wiggles in the curves are due to slight vibrations from the environmental chamber venting liquid Nitrogen into the chamber to keep the temperature at -55°C. I fit all 8 unloading curves and then used

Equations 2 – 7 to calculate the hardness and elastic modulus of the epoxy. The hardness of the epoxy at -55°C is 381 ± 8 MPa and the elastic modulus is 3.74 ± 0.09 GPa.

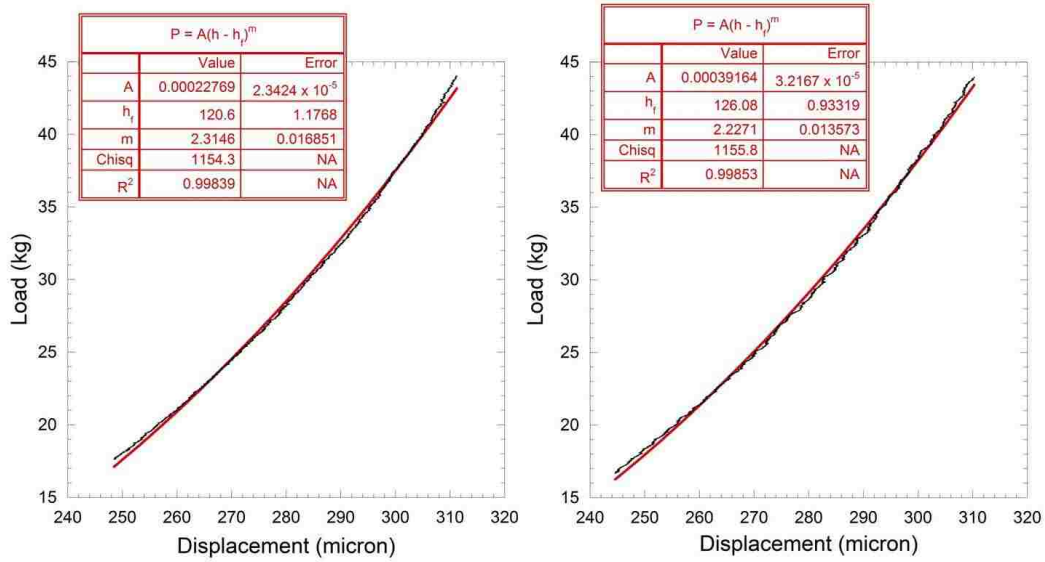

Figure 26. Best fits of Equation 1 to the upper half of the unloading curves plotted in Figure 25.

To evaluate the accuracy of these measurements, I also collected loading and unloading data at room temperature using both the Instron UTM with spherical indenter and a Nanoindenter XP with Berkovich and spherical (D=10μm) indenter tip geometries. Nanoindentation experiments were carried out to a depth of 1 μm, deep enough that the hardness values were near saturation in the case of the spherical tip measurements. The nanoindentation measurement at room temperature is a more trusted approach for calculating material properties using the indentation method [10]. Table 4 is a summary of the results from the Instron UTM and Nanoindenter XP data. The Instron UTM results at room temperature are a little lower than the nanoindentation hardness and elastic modulus. However, the calculation of interfacial fracture energy is not highly sensitive to small changes in the epoxy properties, so the Instron UTM measurements at -55°C were deemed close enough for my purposes.

Table 4. Comparison of hardness and elastic modulus of the bulk epoxy.

Indentation Method	Temperature	Hardness (MPa)	Elastic Modulus (GPa)
Nanoindenter XP Spherical	22°C	263 ± 3	3.82 ± 0.04
Nanoindenter XP Berkovich	22°C	255 ± 2	4.00 ± 0.03
Instron UTM 1/16" SS ball	22°C	195 ± 6	2.87 ± 0.13
Instron UTM 1/16" SS ball	-55°C	381 ± 8	3.74 ± 0.09

5. Interfacial Fracture Energy

5.1. Fracture Mechanics

Fracture mechanics is the study of the propagation of cracks in materials. There are three modes of applying a load to enable a crack to propagate: Mode I fracture (opening/tension), Mode II fracture (sliding/in-plane shear), and Mode III fracture (tearing/out-of-plane shear) [12]. Figure 27 is a diagram showing the three fracture modes. A mix of two or three modes is also possible. Griffith [13] developed a fracture theory based on a simple energy balance. The first law of thermodynamics states that there is a net decrease in energy when a system goes from a nonequilibrium state to equilibrium. Griffith [13] applied this principle to crack formation and reasoned that a crack can only form (or grow) if the process causes the total energy to decrease or remain constant. Therefore, the critical conditions for fracture are defined by crack growth under equilibrium conditions with no net change in the total energy. The Griffith energy balance can be written as [12]:

$$\frac{dT}{dA} = \frac{d\Pi}{dA} + \frac{dW_s}{dA} = 0 \tag{8}$$

$$-\frac{d\Pi}{dA} = \frac{dW_s}{dA} \tag{9}$$

where T is the total energy, Π is the potential energy supplied by the internal strain energy and external forces, and W_s is the work required to create new surfaces. In order for a crack to grow, sufficient potential energy must be available to overcome the surface energy of the material. Consider the plate in Figure 28, which contains a crack of length $2a$, subjected to a constant tensile stress σ. Assume the plate width is >> $2a$ and that

plane stress conditions exist (no out-of-plane stress). Griffith showed that for a linear elastic material [12]:

$$\Pi = \Pi_0 - \frac{\pi\sigma^2 a^2 B}{E} \tag{10}$$

where Π_0 is the potential energy of an uncracked plate, E is Young's modulus (elastic modulus), and B is the plate thickness. The formation of a crack requires the creation of two new surfaces, therefore W_s is given by:

$$W_s = 2A\gamma_s = 4aB\gamma_s \tag{11}$$

where γ_s is the surface energy of the material. Therefore:

$$-\frac{d\Pi}{dA} = \frac{\pi\sigma^2 a}{E} \tag{12}$$

$$\frac{dW_s}{dA} = 2\gamma_s \tag{13}$$

Setting Equations 12 and 13 equal and solving for the fracture stress gives:

$$\sigma_f = \left(\frac{2E\gamma_s}{\pi a}\right)^{1/2} \tag{14}$$

For fracture to occur, the energy stored in the object must be sufficient to overcome the surface energy of the material [12].

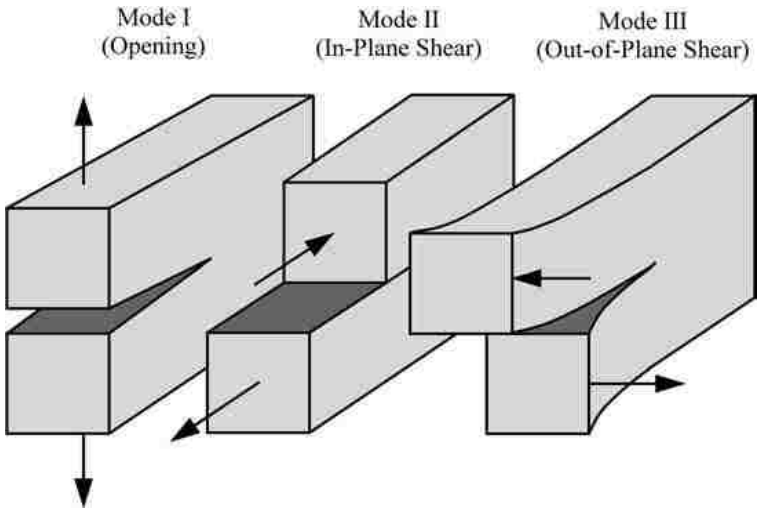

Figure 27. Three modes of loading that can be applied to a crack. Figure is from Anderson [12].

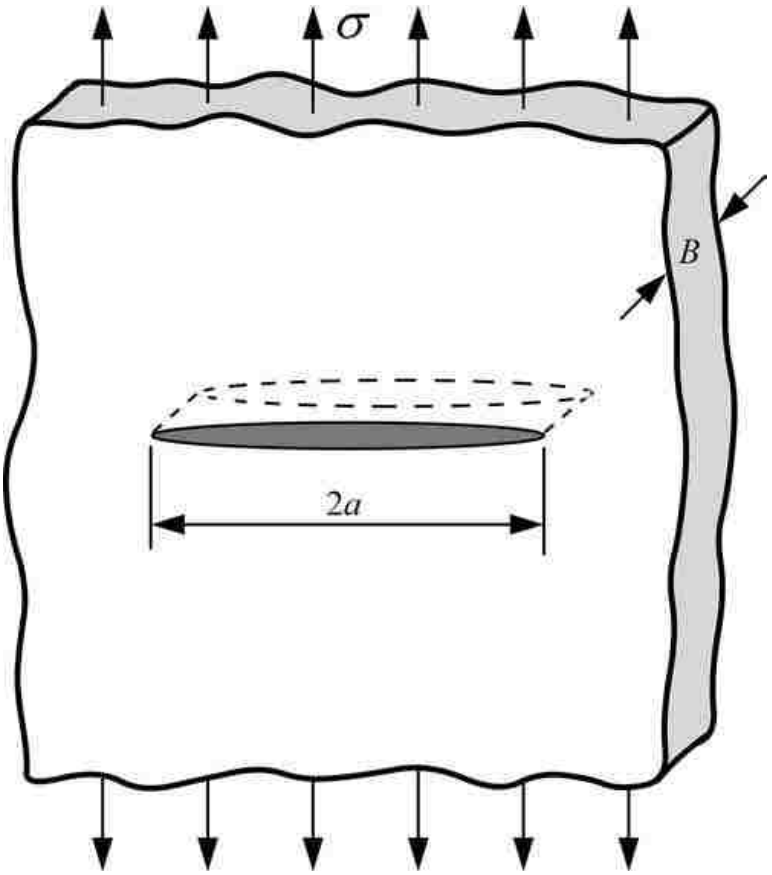

Figure 28. Through-thickness crack in an infinitely wide plate subjected to a remote tensile stress. Figure is from Anderson [12].

Irwin [14] developed an energy approach for fracture that is essentially equivalent to the Griffith model [13] except that it is in a more convenient form for solving problems in engineering. Irwin defined an energy release rate *G* that is a measure of the energy available for an increment of crack growth [12]:

$$G = -\frac{d\Pi}{dA} \tag{15}$$

The term "rate" refers to the rate of change in potential energy that accompanies an increment of crack growth. From Equation 12, the energy release rate for a wide plate in plane stress with a crack of length *2a* is:

$$G = -\frac{d\Pi}{dA} = \frac{\pi\sigma^2 a}{E} \tag{16}$$

Crack growth occurs when G reaches a critical value:

$$G_c = \frac{dW_s}{dA} = 2\gamma_s = \frac{\pi\sigma_f^2 a}{E} \tag{17}$$

where G_c is a measure of the fracture toughness (resistance to fracture/crack growth) of the material. If $G < G_c$, fracture will not occur. If $G \geq G_c$, fracture will occur.

Another parameter used to represent the fracture toughness of a material is the stress intensity factor K. This quantity characterizes the stresses, strains, and displacements near the crack tip in a linear elastic material [12]. The energy release rate G describes the global behavior, whereas K is a local parameter. The stress intensity factor is usually given a subscript to indicate the fracture mode (Figure 27): K_I, K_{II}, and K_{III}. The through-thickness crack in an infinite plate depicted in Figure 28 has Mode I loading (pure tension). Figure 29 shows an element near the tip of a crack in an elastic material with in-plane stresses. The stresses near the crack tip are given by the following equations [12]:

$$\sigma_{xx} = \frac{K_I}{\sqrt{2\pi r}} cos\left(\frac{\theta}{2}\right)\left[1 - sin\left(\frac{\theta}{2}\right) sin\left(\frac{3\theta}{2}\right)\right] \tag{18}$$

$$\sigma_{yy} = \frac{K_I}{\sqrt{2\pi r}} cos\left(\frac{\theta}{2}\right)\left[1 + sin\left(\frac{\theta}{2}\right) sin\left(\frac{3\theta}{2}\right)\right] \tag{19}$$

$$\tau_{xy} = \frac{K_I}{\sqrt{2\pi r}} cos\left(\frac{\theta}{2}\right) sin\left(\frac{\theta}{2}\right) cos\left(\frac{3\theta}{2}\right) \tag{20}$$

For the plate shown in Figure 28 with $\theta = 0$ (the crack plane) and $\sigma_{xx} = \sigma_{yy} = \sigma$, the stress intensity factor is:

$$K_I = \sigma\sqrt{\pi a} \tag{21}$$

The relationship between G and K_I can be seen by comparing Equations 16 and 21:

$$G = \frac{K_I^2}{E} \tag{22}$$

Failure occurs when $K_I = K_{Ic}$ and $G = G_c$. Both K_{Ic} and G_c are assumed to be size-independent material properties [12].

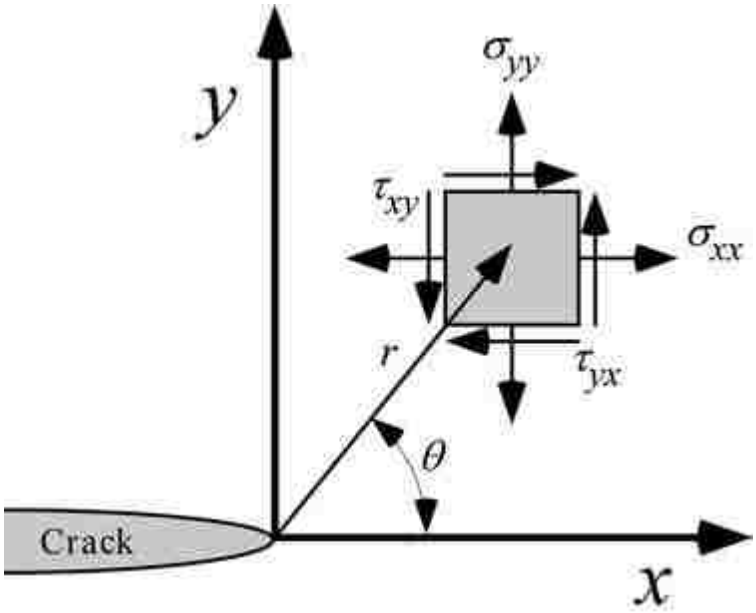

Figure 29. In-plane stresses near the tip of a crack in an elastic material. Figure from Anderson [12].

5.2. Analytical Model

Rosenfeld et al. [5] developed an analytical model for calculating the interfacial fracture energy based on measurements of the delamination size as a function of indenter load. The model is based on a Griffith energy balance approach and assumes that the coating hardness is constant throughout the thickness. The model is applicable to either spherical or Vickers indentation-induced delamination of soft (low elastic modulus) coatings (>10 μm thick) on a rigid substrate. Delamination is driven by contact stresses during loading. The model was developed by modeling the delaminated portion of the coating as an annular plate with plane stress conditions assumed in the radial direction. Figure 30 is a schematic of the annular plate model from Rosenfeld et al. [5]. There is a zero-displacement boundary condition at the outer diameter of the debond crack ($r = c$) due to the surrounding adhered portion of the coating. There is a fixed radial stress σ_{rb} at the inner diameter of the debond crack that is at the outer edge of the contact zone ($r = b$) due to the pressure exerted by the central contact zone. The resulting stress distributions in the delaminated portion of the coating are [5]:

$$\sigma_r = \sigma_{rb} \frac{\left[1+ \alpha c^2/r^2\right]}{\left[1+ \alpha c^2/b^2\right]} \tag{23}$$

$$\sigma_\theta = \sigma_{rb} \frac{\left[1- \alpha c^2/r^2\right]}{\left[1+ \alpha c^2/b^2\right]} \tag{24}$$

where b is the indenter contact radius, c is the debond crack radius, r and θ refer to the radial and circumferential directions, α is $(1 - \nu_e)/(1 + \nu_e)$, and ν_e is Poisson's ratio of the epoxy coating. The strain energy in the plate U is calculated by evaluating the following integral over the volume of the plate [5]:

$$U = \frac{\pi h}{E_e}\int_b^c \left[\sigma_r^2 + \sigma_\theta^2 - 2\nu_e\sigma_r\sigma_\theta\right] r dr \quad (25)$$

where E_e is the elastic modulus of the epoxy coating and h is the coating thickness. The strain energy release rate G is calculated by differentiating the strain energy with respect to crack area [5]:

$$G = \frac{\partial U}{\partial A} = \frac{2(1-\nu_e^2)\sigma_{rb}^2 h}{E_e}\left[\frac{1}{1+\nu_e+(c/b)^2(1-\nu_e)}\right]^2 \quad (26)$$

This is the amount of energy available to form two new surfaces when the coating delaminates from the substrate. Rosenfeld et al. [5] assumed that the coating has a constant hardness, therefore $b = (P/2H)^{1/2}$. P is the indenter load and H is the coating hardness. The vertical stress in the contact zone is the mean indenter contact pressure, which is taken to be the hardness of the coating. The radial stress at $r = b$ is calculated by applying the Tresca yield criteria (max shear stress yield criteria) to the plastically deformed contact zone, resulting in: $\sigma_{rb} = (Y - H)$, where Y is the yield stress of the coating in uniaxial tension. The hardness of the coating is assumed to be 2.25Y, therefore $\sigma_{rb} = -0.56H$. The strain energy release rate can now be expressed in terms of indenter load, rather than indenter contact radius [5]:

$$G = \frac{0.627H^2h(1-\nu_e^2)}{E_e}\frac{1}{[1+\nu_e+2(1-\nu_e)Hc^2/P]^2} \quad (27)$$

This is the critical strain energy release rate for crack propagation G_c, or interfacial fracture energy, when using measured values of delamination sizes as a function of indenter load. If H and G_c are independent of indenter load and crack size, then all parameters in Equation 27 are constants except for P and c. Rearranging terms, we see that P is proportional to c^2, or c is proportional to $P^{1/2}$. Therefore, the slope should be 1/2 when plotting delamination radius c versus indenter load P on a log-log scale.

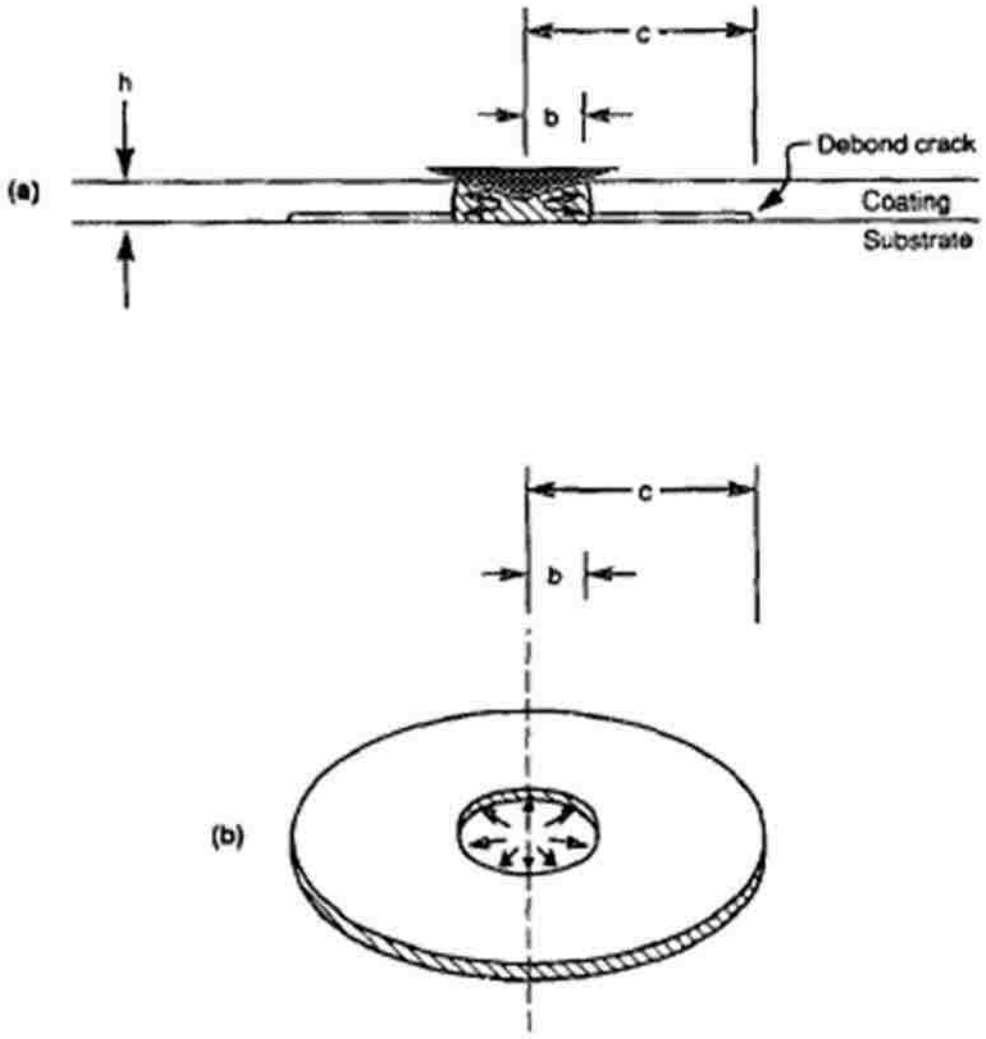

Figure 30. Schematic of Vickers indentation (a) and the annular plate model (b). Figure is from Rosenfeld et al. [5]

To test their model, Rosenfeld et al. [5] performed Vickers indentations at room temperature on soda-lime glass samples with epoxy coatings ranging from 16 to 200 μm in thickness. They had an optical setup to allow them to monitor crack initiation and growth during indentations. Figure 31 shows a sequence of images that they collected as the load was increased and then unloaded. They observed that the debond crack (delamination) forms in an annular region surrounding the central contact zone and

extends stably during the loading portion of the indentation cycle. Crack growth extended in a smooth and continuous fashion as indenter load was increased. There were permanent indent impressions left after unloading, indicating that deformation underneath the indenter was predominately plastic. They measured the hardness of their epoxy coatings of different thicknesses and found that coating hardness was independent of indenter load (Figure 32), which was an assumption they made in their model. Using epoxy properties: H = 238 MPa, E_e = 3.60 GPa, v_e = 0.38, they calculated an average interfacial fracture energy G_c for each coating thickness (Figure 33). They claimed that interfacial fracture energy is independent of coating thickness and reported an overall average $G_c = 25.2 \pm 8.7$ J/m^2.

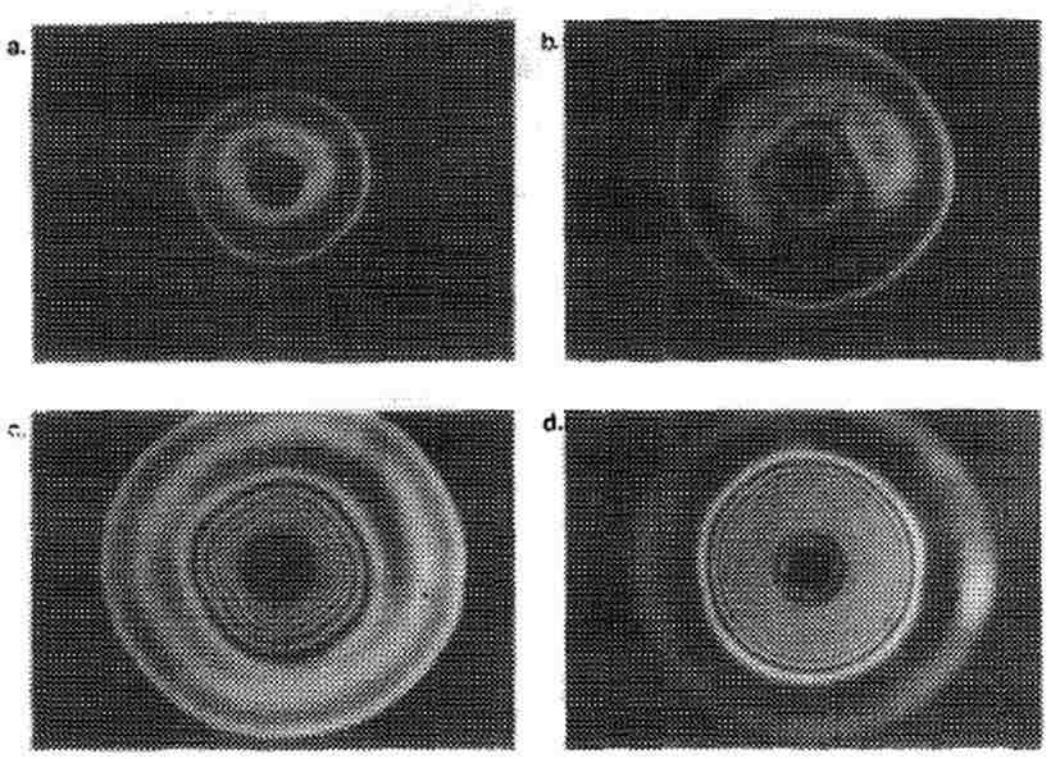

Figure 31. Micrographs illustrating debonding from Vickers indentation at (a) P = 10 N, (b) P = 20 N, (c) P = 30 N, and (d) unloaded. Figure is from Rosenfeld et al. [5].

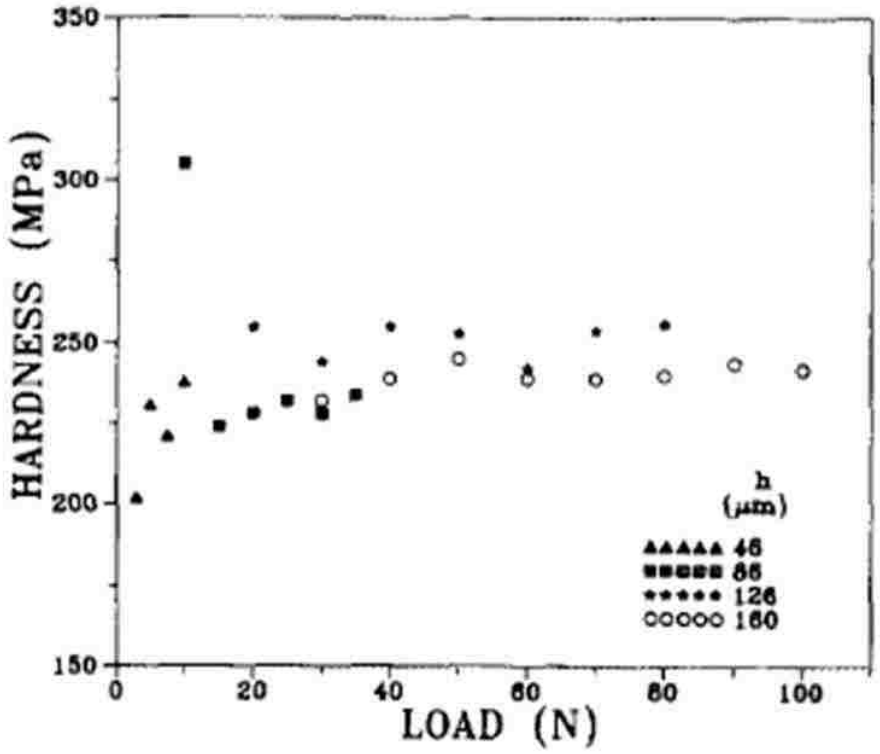

Figure 32. Hardness of epoxy coatings on soda-lime glass substrates as a function of indenter load.

Figure is from Rosenfeld et al. [5].

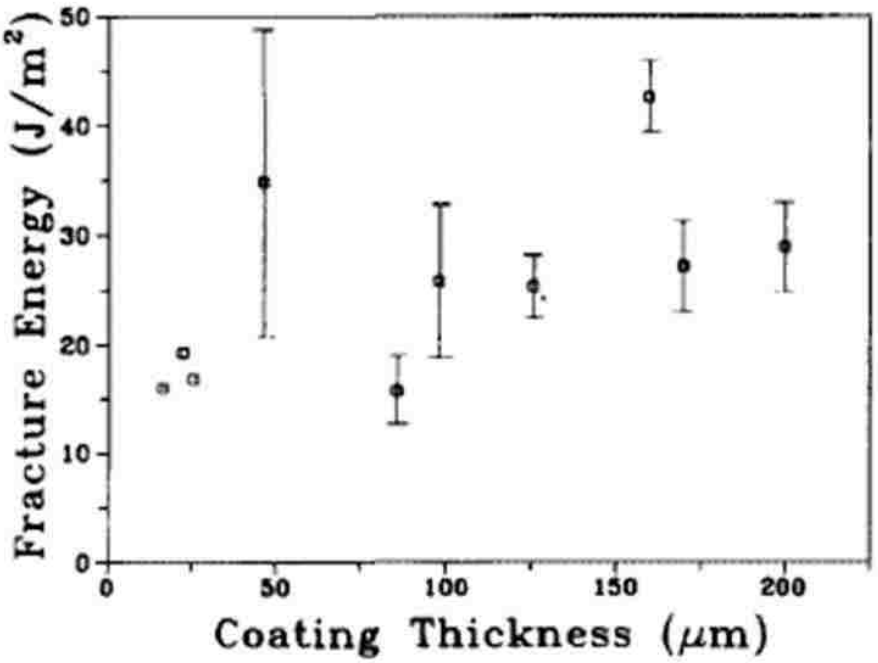

Figure 33. Average interfacial fracture energy with standard deviation for each coating thickness.

Figure is from Rosenfeld et al. [5]

5.3. Analysis of Results

I used Equation 27 and my delamination data from the smooth glass-epoxy coated samples (plotted in Figure 17, excluding indents with glass cracking) to calculate the interfacial fracture energies for both coating thicknesses. The average interfacial fracture energy for the 150 micron coating is $G_c = 368 \pm 68$ J/m^2 and $G_c = 458 \pm 75$ J/m^2 for the 250 micron coating. Although the thicker coating has a higher average G_c, there is overlap between the two groups (Figure 34). Rosenfeld et al. [5] stated that interfacial fracture energy is independent of coating thickness. It is unclear whether or not my data support this assertion, since I only studied two coating thicknesses. From the right side of Equation 27, we see that all parameters are constants except h and c^2/P (h = coating thickness, c = crack/delamination radius, P = delamination load). If c^2/P is also a constant, then G_c is dependent on coating thickness h. Figure 35 is a plot of c^2/P versus delamination load. The average c^2/P is higher for the thicker coating. However, there is scatter in the data and a horizontal line could be drawn through all the data (both coating thicknesses) at about 3900 μm^2/N (pink line in Figure 35). Therefore, it remains unclear whether my data support the claim by Rosenfeld et al. [5] that interfacial fracture energy is independent of coating thickness. Calculating an overall average G_c for both coating thicknesses results in $G_c = 420 \pm 84$ J/m^2. Rosenfeld et al. [5] calculated an average $G_c = 25.2 \pm 8.7$ J/m^2 for a similar soda-lime glass-epoxy coated system, an order of magnitude lower than my calculation. Rosenfeld et al. [5] used different epoxy properties, since their experiments were done at room temperature. Using their epoxy properties (H = 238 MPa, E = 3.60 GPa, ν = 0.38) with my delamination data results in an average $G_c = 273 \pm 53$ J/m^2, which is lower than the average G_c that I calculated using my epoxy properties (H =

381, E = 3.74, ν = 0.4) but still an order of magnitude higher than the Rosenfeld [5] value. The reason their interfacial fracture energy is so much lower is because they detected delaminations at extremely low loads. Rosenfeld et al. [5] observed crack initiation at loads less than 1 kg. Then they grew the delamination as the load increased to about 10 kg. My samples required much higher loads for crack initiation and the crack would suddenly "pop-in" rather than start out tiny and grow in a stable fashion. I did additional experiments on a 150 micron epoxy coating at 10, 15, and 20 kg (5 indents at each load) to see if there was any hint of delamination. The results are shown in Figure 36. There were no indent impressions on the surface; the deformation was completely elastic. There appears to be a hint of something going on, but it does not look like delamination. It was difficult to get good images because the white regions are so faint and diffuse. Cross-polarized light (which is why there is a cross though the center of the images) worked the best. It is unclear if the fuzzy white areas could be stress in the epoxy, where bonds are stretching without breaking, but it does not appear to be delaminations. The images look nothing like my delaminations or the delaminations that Rosenfeld et al. [5] imaged (Figure 31). It is not clear why they had delaminations at such low loads, but it is evident that my samples have significantly better adhesion than theirs.

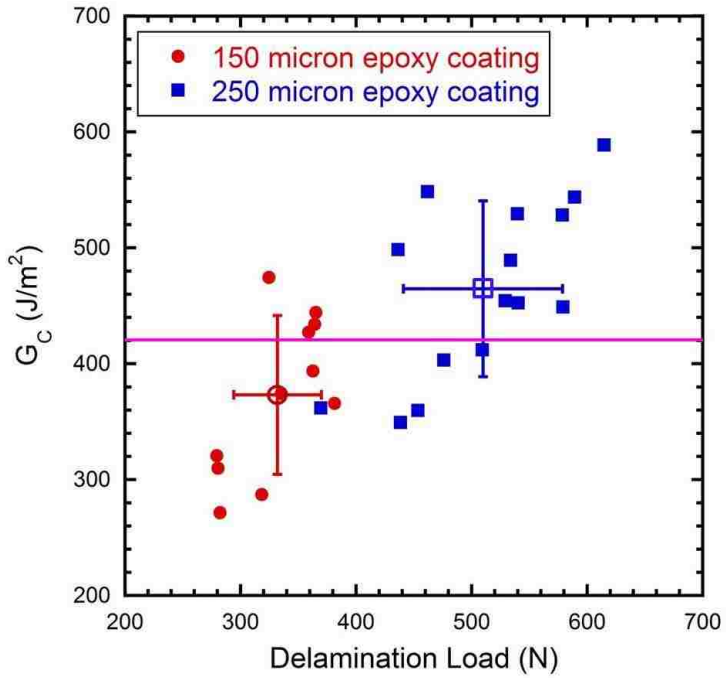

Figure 34. Interfacial fracture energies (G_c) for both 150 and 250 micron epoxy coatings. The average values with error bars denoting standard deviations are also plotted. The pink line indicates the overall average for both coating thicknesses.

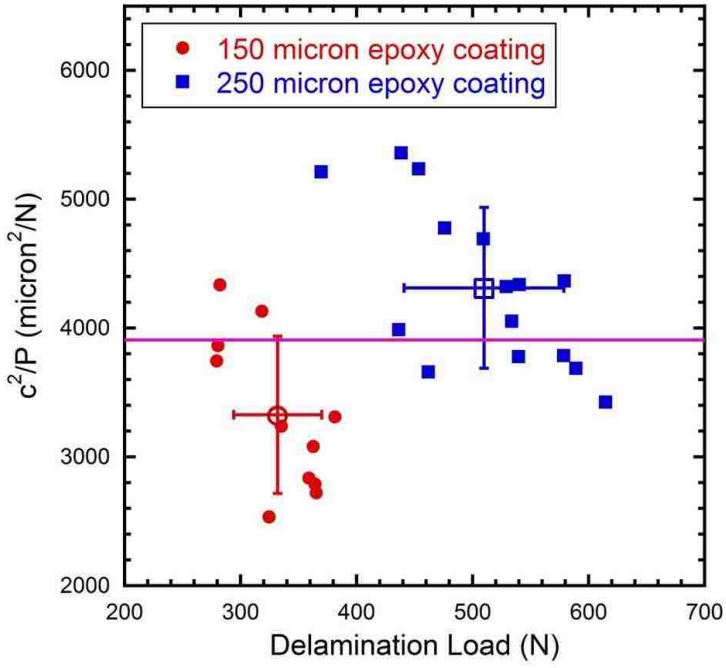

Figure 35. Plot of c^2/P versus delamination load for both 150 and 250 micron epoxy coatings. The average values with error bars denoting standard deviations are also plotted. The pink line indicates the overall average for both coating thicknesses.

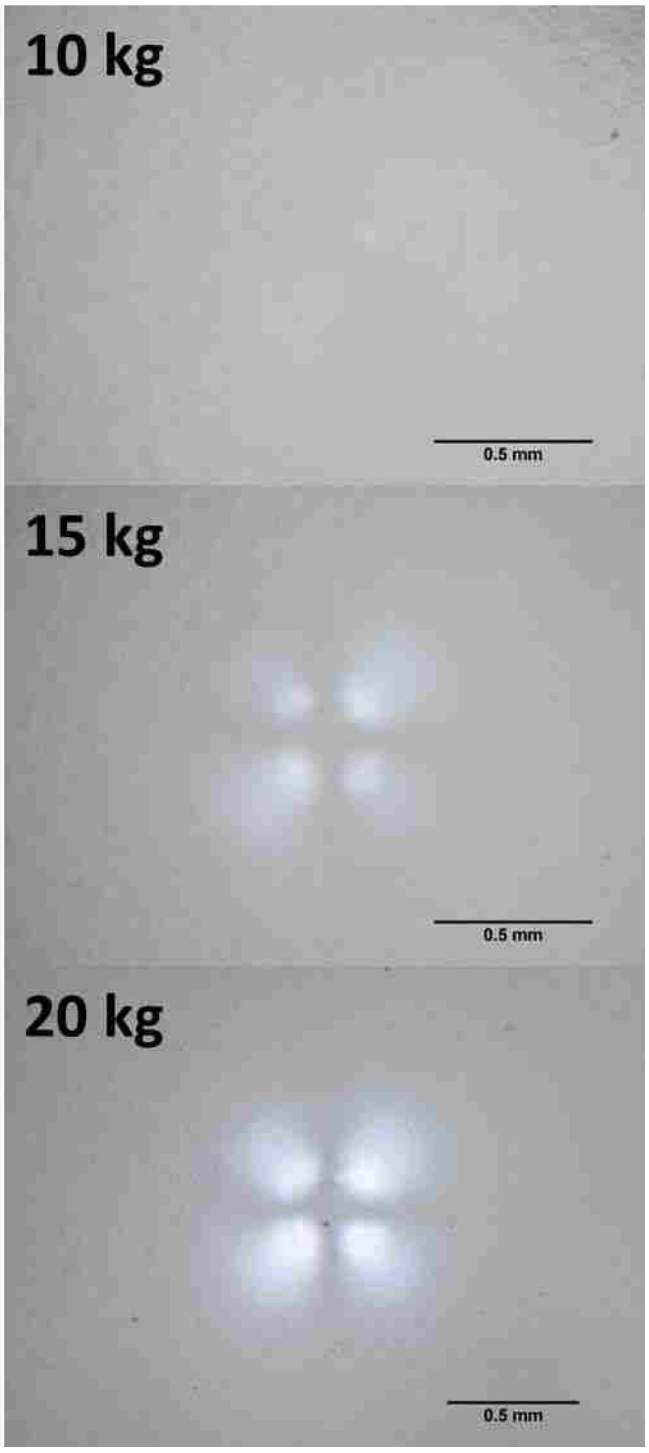

Figure 36. Cross-polarized light images of indentations performed at low loads.

I also calculated the interfacial fracture energy for the other glass samples that I tested (rough, stressed, uncleaned). The results are summarized in Table 5 and plotted in

Figure 37. The glass samples with mold release have a high degree of variability (large standard deviations). It is also clear that the rough glass samples have a much higher interfacial fracture energy than any of the other samples. The rest of the glass samples all cluster around $G_c \approx 400$ J/m^2, which is consistent with the average interfacial fracture energy that I calculated using only the smooth, non-stressed, clean samples ($G_c = 420 \pm 84$ J/m^2). Although the uncleaned and stressed samples delaminate at lower loads, the interfacial fracture energy is similar to the clean, non-stressed samples. This is because the delamination sizes are smaller for the uncleaned and stressed samples (lower delamination load = smaller delamination size). These data suggest that G_c is independent of coating thickness (as stated by Rosenfeld et al. [5]), since both the 150 and 250 micron data have similar interfacial fracture energies. Using the Vickers indentation data plotted in Figure 20 results in $G_c = 422 \pm 43$ J/m^2, also consistent with the overall average.

Table 5. Comparison of interfacial fracture energies for the different glass samples that were tested.

150 micron epoxy coating	Average G_c (J/m^2)	Standard Deviation (J/m^2)
Smooth, Non-stressed, Clean	368	68
Dirty	407	27
Mold Release	316	118
Stressed	365	62
Rough	1097	188
250 micron epoxy coating		
Smooth, Non-stressed, Clean	458	75
Dirty	382	55
Mold Release	395	305
Stressed	357	76

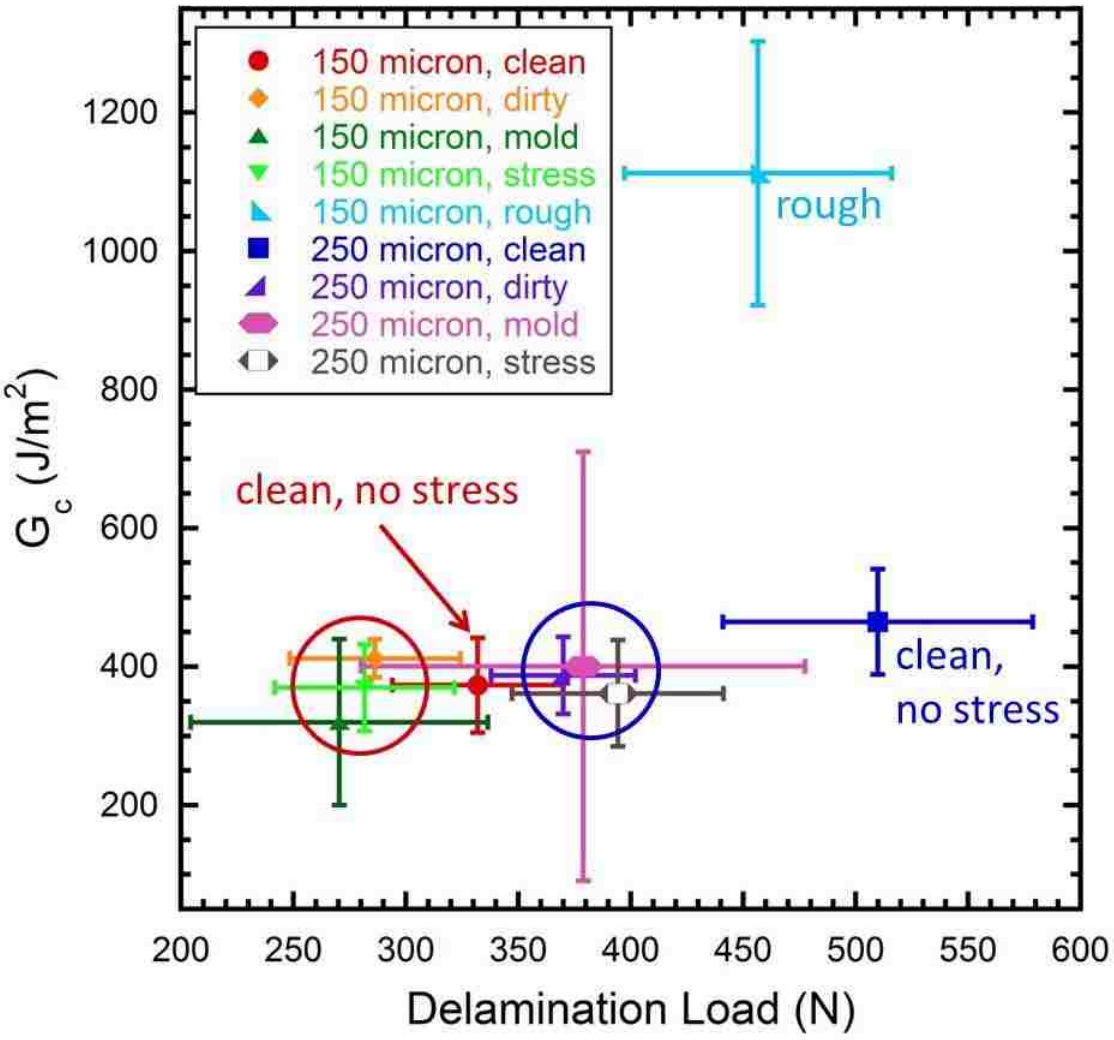

Figure 37. Interfacial fracture energies for the different glass samples that were tested. The circles indicate the dirty, mold release, and stressed samples for each coating thickness.

As explained in the previous section, the Rosenfeld [5] model predicts a *c* versus $P^{1/2}$ dependence. Therefore, the slope should be 1/2 when plotting delamination radius versus indenter load on a log-log scale. Figure 38 shows my results, along with the results from Rosenfeld et al. [5] for comparison. It is clear that both data sets follow the expected trend of slope 1/2. However, my data plot to the right of Rosenfeld et al. [5] because my samples require at least three times the load in order to initiate delamination. The fact that

my data follow the slope 1/2 trend suggests that even though I introduced a residual thermal stress by doing the experiments at cold temperature, the model is still applicable.

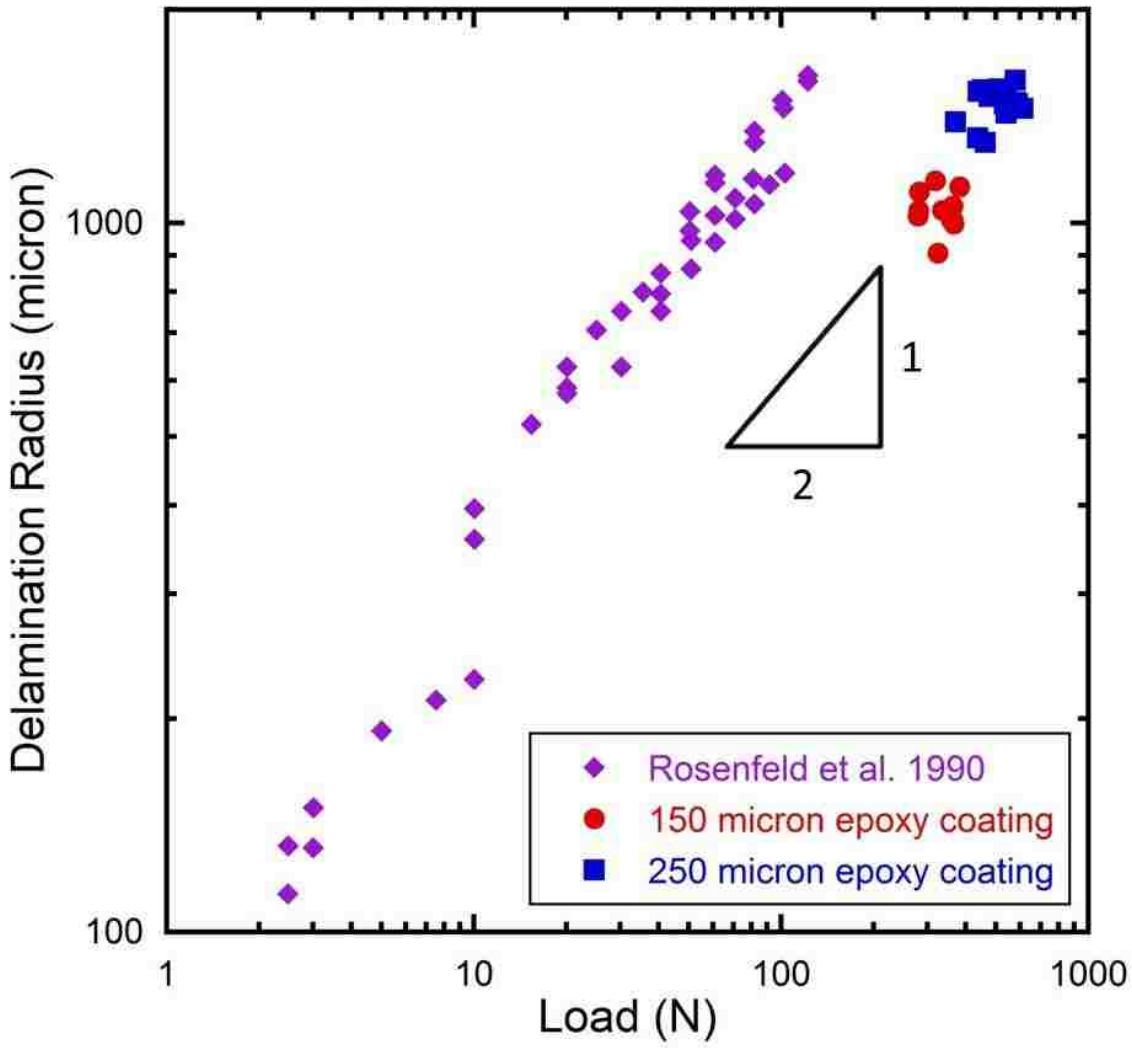

Figure 38. Log-log plot of delamination radius as a function of indenter load for both 150 and 250 micron data. The data from Rosenfeld et al. [5] is included for comparison.

6. Conclusions

Typically, the Oliver and Pharr method is applied to nanoindentation data. I have applied this method to Instron UTM load-displacement data to estimate the hardness and elastic modulus of bulk Epon 828/DEA epoxy at room temperature and -55°C. I have also utilized the indentation method at -55°C to induce delamination of an epoxy coating from a glass substrate. The measured delamination radii and loads were used to calculate an interfacial fracture energy of $G_c \approx 400$ J/m^2 for a soda-lime glass-epoxy coated system, an order of magnitude higher than a similar study by Rosenfeld et al. [5]. My results demonstrate that using an Instron UTM modified for indentation is a viable means to calculate the hardness and elastic modulus of a soft material, as well as the interfacial fracture energy of a soft coating on a rigid substrate. The benefit of using an Instron UTM, versus a Nanoindenter, is that larger samples can be tested and much higher loads can be attained. The addition of an environmental chamber allows a range of temperatures to be accessible.

Applying the Rosenfeld [5] model to Instron UTM delamination data is a simple means to quantitatively measure the adhesion of a soft coating to a rigid substrate. The indentation method can also be used qualitatively to compare the adhesion of different samples. For example, varying amounts of silane (an adhesion promoter) can be added to the epoxy. Or the surface of the substrate could be roughened to varying degrees. The delamination sizes can then be compared to determine which sample has better adhesion. This methodology can be employed to test and refine sample processing procedures. The indentation method is a simple technique to measure adhesion, either quantitatively or qualitatively.

References

[1] A. J. Kinloch, Adhesion and Adhesives, London: Chapman & Hall, 1987.

[2] J. Chen and S. J. Bull, "Approaches to investigate delamination and interfacial toughness in coated systems: an overview," *Journal of Physics D: Applied Physics,* vol. 44, no. 3, pp. 1-19, 2011.

[3] R. Lacombe, Adhesion Measurement Methods: Theory and Practice, Boca Raton: Taylor & Francis Group, 2006.

[4] M. R. Lin, J. E. Ritter, L. Rosenfeld and T. J. Lardner, "Measuring the interfacial shear strength of thin polymer coatings on glass," *Journal of Materials Research,* vol. 5, no. 5, pp. 1110-1117, 1990.

[5] L. G. Rosenfeld, J. E. Ritter, T. J. Lardner and M. R. Lin, "Use of the microindentation technique for determining interfacial fracture energy," *Journal of Applied Physics,* vol. 67, no. 7, pp. 3291-3296, 1990.

[6] J. E. Ritter, T. J. Lardner, L. Rosenfeld and M. R. Lin, "Measurement of adhesion of thin polymer coatings by indentation," *Journal of Applied Physics,* vol. 66, no. 8, pp. 3626-3634, 1989.

[7] G. Tang, Y.-L. Shen, D. Singh and N. Chawla, "Indentation behavior of metal-ceramic multilayers at the nanoscale: Numerical analysis and experimental verification," *Acta Materialia,* vol. 58, pp. 2033-2044, 2010.

[8] P. D. Warren, D. A. Hills and D. N. Dai, "Mechanics of Hertzian cracking," *Tribology International,* vol. 28, no. 6, pp. 357-362, 1995.

[9] W. C. Oliver and G. M. Pharr, "An improved technique for determining hardness and elastic modulus using load and displacement sensing indentation experiments," *Journal of Materials Research,* vol. 7, no. 6, pp. 1564-1583, 1992.

[10] ASTM Standard E2546-07, "Standard Practice for Instrumented Indentation Testing," ASTM International, West Conshohocken, PA, 2007.

[11] A. C. Fischer-Cripps, Nanoindentation, Third ed., F. F. Ling, Ed., New York: Springer, 2011.

[12] T. L. Anderson, Fracture Mechanics: Fundamentals and Applications, 3rd ed., Boca Raton: Taylor & Francis Group, 2005.

[13] A. A. Griffith, "The phenomena of rupture and flow in solids," *Philosophical Transactions of the Royal Society of London, Series A,* vol. 221, pp. 163-198, 1920.

[14] G. R. Irwin, "Onset of fast crack propagation in high strength steel and aluminum alloys," *Sagamore Research Conference Proceedings,* vol. 2, pp. 289-305, 1956.